MICROFLUIDIC PLATFORMS FOR INVESTIGATING CELLULAR GROWTH AND SUB-CELLULAR COMPONENT SEPARATION

A Thesis

by

RAVI CHAWLA

Submitted to the Office of Graduate and Professional Studies of
Texas A&M University
in partial fulfillment of the requirements for the degree of

MASTER OF SCIENCE

Chair of Committee,	M. Nazmul Karim
Committee Members,	Victor M. Ugaz
	Hung-Jen Wu
Head of Department,	M. Nazmul Karim

May 2016

Major Subject: Chemical Engineering

ABSTRACT

A static droplet array was used for growth investigation of single-and multiple cells of two *Saccharomyces cerevisiae* strains (FY2 and SM14/P1A2). The observed encapsulation efficiency for single cells was 36.4% which was close to the random encapsulation efficiency of 28.9%. For the SM14/P1A2 strain, we observed an average specific growth rate of 0.236 hr^{-1} in YNB media and for the FY2-GFP strain we observed an average growth rate of 0.257 hr^{-1}. The results for the P1A2 strain from the droplet experiment were comparable with the results from the bioreactor studies of the strains. In addition to the static droplet array, we also investigated a perfusion chip to understand the growth heterogeneities of *Chlorella vulgaris* single and multiple cells. Cell growth can be monitored for multiple days, with preliminary results showing good qualitative agreement between growth and size distributions obtained in bulk and in droplet experiments.

We also studied the enzymatic etching of poly(lactic acid) (PLA) substrates to obtain nano- and micron sized channels. The aim of the project was to etch channels separated by a weir of height in the sub-micron range, enabling the possible separation of sub-cellular components. Characteristic etch rates of 1.45 μm h^{-1} and 0.16 μm h^{-1} for the poly(lactic acid) at 37°C and 24.4°C using the enzyme proteinase K were obtained. Lower temperature (24.4°C) provided a better control over etch depths of the channels at sub-micron scale. The proposed architecture with the weir depth in the sub-micron range could be used for separation of sub-cellular components like exosomes.

DEDICATION

To family and friends.

ACKNOWLEDGEMENTS

I would like to thank my committee chair, Dr. Karim, and my committee members, Dr. Ugaz and Dr. Wu, for their guidance and support throughout the course of this research.

Thanks also go to my friends and colleagues and the department faculty and staff for making my time at Texas A&M University a great experience. I also want to extend my gratitude to the National Education Foundation and the Texas A&M Engineering Experimental Station for the financial support.

Finally, thanks to my family and friends for their unwavering support, encouragement and faith in me.

NOMENCLATURE

C. vulgaris	*Chlorella vulgaris*
CFD	Computational Fluid Dynamics
EV	Extracellular vesicles
Mtb	*Mycobacterium tuberculosis*
PDMS	poly(dimethyl siloxane)
PLA	poly(lactic acid)
S. cerevisiae	*Saccharomyces cerevisiae*
TB	Tuberculosis

TABLE OF CONTENTS

Page

LIST OF FIGURES

Page

LIST OF TABLES

Page

1. INTRODUCTION

Over last two decades there has been a rapid growth in the microfluidic applications primarily because it is easy to manipulate and control the flow of fluids at micron length scale. [1-3] The ability to precisely control the flow of the fluid paves way for easier manipulation and better understanding of the cell growth, and thus has been especially helpful in advancing the field of the biology [4]. Microfluidics is also being explored for health care for diagnostics purposes and has the potential to revolutionize the health care scenario across the globe [5]. Not only can microfluidics help in better, effective and faster diagnostics, it can potentially make diagnostics available at a decreased cost to millions of people in developing countries. [6] Microfluidics with its diverse applications and potential is a truly multi-disciplinary endeavor with researchers involved from applied sciences to various branches of engineering [7].

In this work, we explored microfluidics to investigate the growth kinetics of single-cell and multiple cells in PDMS-based devices in droplets and continuous microfluidic mode. Previous work by Dewan et al.[8] formed the basis of this work. Another area that was explored in this work is sub-micron etching of Poly (lactic acid) devices using Proteinase-K enzyme. The work reported here is continuation of the original work by Huang et al. [9] The intended application of the etched substrate for this work was to achieve high-throughput separation of sub-micron particles from a mixture of differently sized particles, for e.g. for separation of sub-cellular components like extracellular vesicles from protein, cell debris, and other cellular components.

2. BACKGROUND & LITERATURE REVIEW

2.1 Cell growth in microfluidic droplets

There has been an increased interest in industry to exploit microbes such as algae and yeast for biofuels and nutraceuticals like β-caratenoid, etc. [10] There is also a huge interest in yeast cells like *S. cervisiae* for production of ethanol [11], n-butanol [12], carotenoids [13] and other important compounds. For a successful venture in the field, it is vital to identify strains, environmental conditions for rapid growth and cellular phenomena, which controls the final product (for e.g. lipid content in case of algae and β-carotenoid in the case of yeast). To understand the impact of culturing techniques on cellular growth phenomena, it is important to understand how microenvironment around a cell impacts the physiological cell response to chemical and physical stimuli. Genetic modification, chemical stimuli (like metabolite concentration, pH, carbon source, substrate composition and concentration, oxygen) and physical stimuli (like temperature, light, electrical charges, flow rates and shear stresses experienced by cells) can significantly alter cell growth and division [8,14-17]. It is critical to investigate the impact of such modifications on physiological response of cell and microfluidic devices provide the tools to investigate it the resolution of single-cell.

Several tools such as bioreactors [13], flow cytometer [18], microwell plates [19] exist to monitor the bulk growth of cells but tools provide an average response of billions of cells and losing the heterogeneity of the population [15]. Bioreactor is one of the most commonly used method to establish the kinetic parameters quantified by

measurement of optical density/biomass/ cell number in representative samples collected from the bioreactor. These kinetic parameters measured from such an approach represent a statistical average of the properties of all the cells and hence, bioreactor-based approach losses the individual growth kinetics of individual cells and its descendants. Flow cytometer [18] is another common tool used for sorting cells, determining cell size, and identifying intracellular organelles. Despite being able to track a large number of cells, flow cytometer only allows for end-point measurements of a cell and does not allow for tracking the changes in the cell and its progeny over time. Microwell plates is yet another commonly used technique to monitor the growth of cells but present difficulty in isolating single cells in wells [20].

Microfluidic methods with their ease of manipulation of small volumes can be employed to easily track and understand the single-cell growth and heterogeneities, which is not possible in bulk culturing techniques. Current microfluidic devices for single-cell analysis (SCA) can be divided into invasive and non-invasive single-cell analysis, where non-invasive single-cell analysis could be further divided into time-resolved and time resolved [16]. A detailed review of the advantages, disadvantages and challenges of these microfluidic devices is presented in Ref [16].

Droplet-based microfluidics is an attractive platform to investigate cellular phenomena. [15,21] Droplets can be used for rapid encapsulation of single, double and multiple cells in high-throughput fashion and presents a time resolved non-invasive strategy for investigating cellular growth [22,23]. Immobilized droplets are used to study the growth kinetics of individual cells, and cells and their progeny can be monitored over

a long period of time, and thus act as miniaturized ‘batch’ bioreactors [8,24,25]. Such microfluidic platforms with their small footprint makes it fairly easy to expose all the droplets, and consequently cells to the same environmental conditions like light and temperature. Several studies have exploited microfluidic droplets for analysis of single cells including mammalian [26,27] , yeast [28,29], bacteria [30] and algal cells [24,31,32].

Polydimethylsiloxane (PDMS), a biocompatible and optically transparent material, is a popular material for microfluidic applications. However, droplet-based microfluidics encounters challenge in terms of droplet storage in these PDMS devices because of its porosity to small molecules [33]. The water-diffusion through PDMS can change the size (shrinkage in this case) of the droplet over time and ultimately the droplet would no longer be a constant volume batch system [34]. The challenge of droplet shrinkage in PDMS devices can be addressed by saturating PDMS with water using a water reservoir around the device. [25,35]

The challenge to achieve a long-term storage of the droplet for this work was addressed by Dewan et al [8] by modifying storage method reported by Shim et al. [34] A thin PDMS membrane was used as a bottom layer of the device (instead of a glass slide), and placing this assembly in a water reservoir. [8,34] This strategy allows the water that escapes because of PDMS porosity to be replenished by the water that diffuses through the thin layer at bottom. The work demonstrated droplet storage for more than 30 days without significant shrinkage of droplet and showed the growth of single and multiple *C. vulgaris* cells. [8]

This study is based on the work of Dewan et al [8] and droplet-based microfluidics is employed to isolate individual cells of yeast in droplets (of nanoliter-volume range) in a well-defined microenvironment. Specifically, the aim of this work was to investigate the growth kinetics of *S. cervisiae* at the level of single or few cells and to relate the growth parameters to changes in cell size distribution

2.2 Perfusion chip for algal cells

Biofuel from microalgae is being explored as a potential alternative to conventional oil and is currently believed to be the most feasible renewable technology to meet future demands [36]. The production of oil from microalgae would require identification of the strains that inherently produce or could be engineered to produce the maximum amount of lipids in the shortest cultivation time. Naturally fast growing algal strains might not be the algal strains with most lipids, and hence genetic engineering of cells needs to be explored. Single cell studies can provide a wealth of fundamental information of cell physiology like growth rates, biomass, and impact of genetic modification, understanding of which would greatly impact the bulk harvesting techniques. Therefore, to harvest the full potential of an industrial scale culture (lipids in case of algae, carotenoid in case of yeast), it becomes critical to understand the differences in single cell growth under different cultivation conditions. Microfluidic devices provide a precise spatio-temporal control over the cell microenvironment and hence are a useful tool to conduct studies to investigate the responses of single cells that could lead to better prediction and control of bulk cultures.

In previous work, Dewan et al [8] investigated the growth kinetics and size distribution of single and multiple algal cells (*Chlorella vulgaris*) in a static droplet array. The work noted that *Chlorella vulgaris* does not follow the typical doubling hypothesis and found that *C. vulgaris* cells divide into 3, 4 and 5 daughter cells. *Chlorella vulgaris* grows by autosporulation and work of Yamamoto et al [37] had shown a variable number of daughter cells per autosporangium (2, 3, 4, 6, 8, 16 and 32 daughter cells per autosporangium). This heterogeneity in cell growth leads to a heterogeneity noted in specific growth rate of single and multiple *C. Vulgaris* cells. In their later work Yamamoto et al [38] demonstrated that the algal cell cycle involved two processes: cell growth and cell division, where cell division could be further sub-divided into following phases: chloroplast division, first protoplast division, second protoplast division, autospore maturation, and lastly hatching of the autospores. To get a better understanding of the growth kinetics and cell division, we tested a set of experiments to observe the growth of single and multiple algal cells in a perfusion chip where the cells grow without being nutrient limited. Conditions like these would be characteristic of a macro-scale continuous bioreactor setup where nutrients are being constantly supplied to the cells. We were interested in understanding the heterogeneity of cell division and if the daughter cells showed similar heterogeneous cell division. In addition, we were interested how lipid content of single cell changes over its growth cycle.

2.3 Enzymatically etched PLA devices for sub-micron particle separation

Enzymatic micromachining [9] provides a micro-fabrication method that harnesses the chemical activity of enzymes on a biodegradable substrate and thus etches nano-and microchannels. Huang et al [9] demonstrated coordinated patterning and machining by manipulating the interaction between enzyme, substrate and an enzyme inhibitor and used it to fashion membrane-less filter geometry for cell separation experiments. For the experiments in the work enzyme Proteinase-K [PK], acted on the Poly (lactic acid) (PLA) substrate in presence of enzyme inhibitor Bovine Serum Albumin (BSA). The etching is achieved by flow of the enzyme PK on PLA substrate using microfluidic template created using soft lithography. The enzyme flow imprinted a replica of flow path into the substrate on the floor. The enzymatic reaction, a surface reaction, like any other chemical reaction, depends on the concentration of enzyme, duration of the reaction, and temperature of the reaction (Figure 1). The etch depth on the substrate thus could be manipulated by varying the enzyme concentration, time and temperature of the etching.

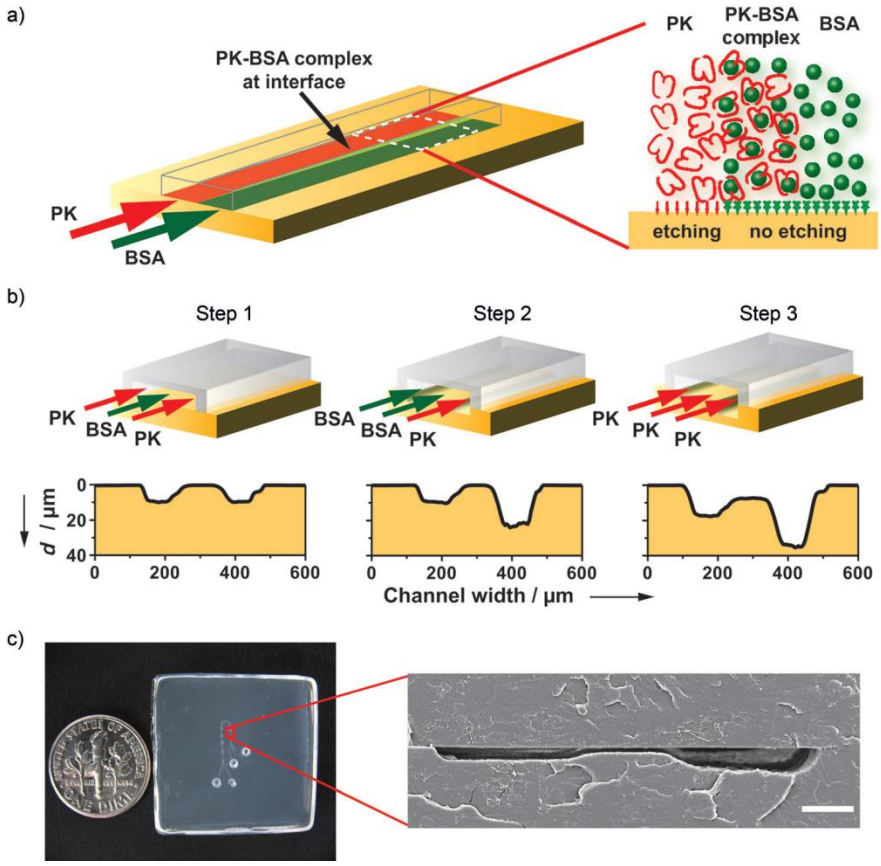

Figure 1. Enzymatic micro-machining of the PLA substrate. [9]

In the work, a membrane-less filtration architecture for separation of cancer cells was patterned by addition of BSA (an enzyme inhibitor) to selectively etch portions of the substrate. The binding between proteinase K and the BSA protein inactivates the lateral diffusion of the enzyme and the boundary of the etched region was thus sharply defined. Additionally, size of the etched zone could be manipulated by varying the BSA concentration, which consequently varied the lateral diffusion driving force with respect to the adjoining PK stream. This mechanism was be exploited to construct micro-channels incorporating weir-like barriers oriented parallel to the flow direction by

sequentially varying the composition in each stream i.e. this technique was used to fabricate a microfluidic architecture incorporating an embedded weir-like barrier. This flow-architecture has two driving forces for transportation of smaller-sized components across the barrier from inner lane to outer lane (Figure 2):

i. Curved flow path leading to dean vortices (secondary transverse motion)

ii. Unequal depths created a pressure gradient (and velocity gradient) across the barrier.

Curvature-induced forces (Dean vortices) permited the filtration barrier to be oriented parallel to the flow direction rather than perpendicular to it, thus avoiding clogging and minimizing the pressure drop.

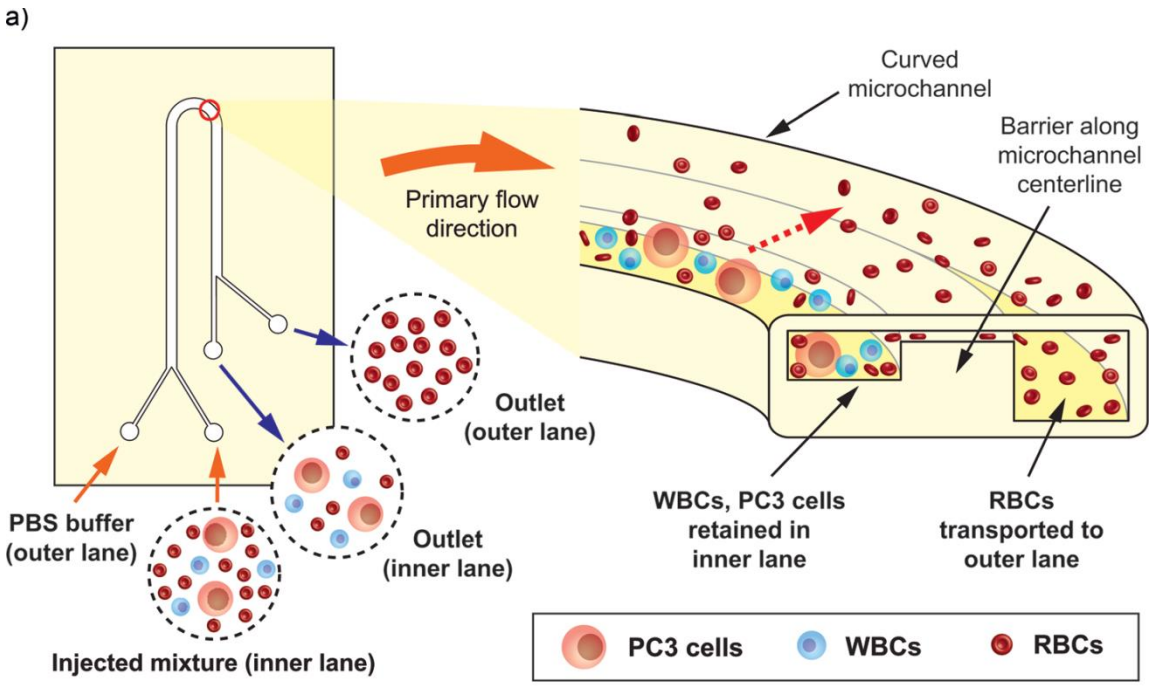

Figure 2. Membrane-less architecture for high-throughput separation of PC3 cancer cells and blood cells. [9]

This architecture was shown to effectively separate rare cells from whole blood in a continuous, high-throughput operation and order of magnitude faster than currently used separation methods. This architecture consequently provides the basis for an effective and high-throughput separation of smaller-sized components from larger sized components. Huang et al. [9] also reported a characteristic etch rate of 2 micron/h and reported creating nano-channel of depth 170 nm-deep channel by injection of a PK solution at 2 mL/min for 3 h at room temperature.

In their original work emphasis was paid on separating different sized cells (PC3 cancer cells ~20 micron and RBC cells ~6 micron). The separation, however, is not just limited to cell-sized bodies and can be used to separate smaller sub-cellular components

from other larger sub-cellular and cell-sized components. This hypothesis forms the basis of the current work and an effort is made to fabricate a device that would enable separation of sub-cellular components known as extracellular vesicles (EVs). Also, in this work the fabrication procedure has been altered to eliminate the need of the enzyme inhibitor.

Extracellular vesicles (EVs), vesicles released by variety of cells in different extracellular spaces, are of special interest from a separation point of view. EVs serve as vehicles for transfer between cells of membrane and cytosolic proteins, lipids and RNA and thus play important role in cell-to-cell communication communication[39]. Cells secrete these vesicles in different extracellular spaces, including, blood, urine, saliva, amniotic fluid, etc. EVs comprise of exosomes (40-100nm) and microvesicles (>1μm), and are membrane vesicles of endosomal and membrane origin respectively. [39] Recently, EVs have garnered a lot of attention and investigation in the last decade for the potential applications in the field of medical diagnostics and therapeutics. EVs can serve as important biomarkers for early detection of cancer [40], HIV [41], tuberculosis [42,43] etc. The discovery of machinery regulating the vesicular traffic inside the cell won the Nobel Prize in Medicine 2013.

Tuberculosis (TB), caused by the bacillus *Mycobacterium tuberculosis* (Mtb), is one of the world's deadliest communicable diseases. The 2014 World Health Organization's Global Report on Tuberculosis [44] reported that an estimated 9.0 million people developed TB and 1.5 million died in the year 2013. Thus, exosomes and microvesicles released from *Mtb* infected macrophages are of a special interest. [45-48]

In this work we extend the application of the work [9] to make an attempt to separate sub-micron cellular components like microvesicles and exosomes.

3. MATERIALS AND METHOD

3.1 Design of static droplet array

The fluidic network in the device comprises of a repeated sequence of loops, where each loop has two branches with the lower branch containing a hydrodynamic trap [49]**.** The upper branch is a rectangular channel with uniform width (200μm), and the lower branch was divided into four sections: three rectangular sections (100μm each) and the circular section, served as the hydrodynamic trap (385μm), the device had a uniform height 80μm (Figure 3). The ratio of the hydrodynamic resistances of the lower to upper branch resistance was 0.78231, and the calculations involved are depicted in Table 1 and Table 2.

The tables also show the variation of the ratio of the resistance for two different trap diameters. As can be seen the ratio can varied by varying the width and length of the constriction in the hydrodynamic trap and, the length of the upper branch [49]. The channel resistances R_l and R_u were calculated using the exact analytical solution of Poiseuille flow in a rectangular channel along each path from measured geometry dimensions. f and R were given by Equation 1 and 2 respectively, and the calculations for trap radius of 385 μm and 400 μm are presented in Table 1 and Table 2.

$$\mathbf{f} = \sum_{\mathbf{n,odd}}^{\infty} \frac{\mathbf{1}}{\mathbf{n^5}} \times \frac{\mathbf{192}}{\boldsymbol{\pi}^{\mathbf{5}}} \times \frac{\mathbf{h}}{\mathbf{w}} \mathbf{tanh}\left(\frac{\mathbf{n\pi w}}{\mathbf{2h}}\right) \qquad \text{Equation 1}$$

$$\mathbf{R} = \frac{\mathbf{12\mu L}}{\mathbf{h^3 w}}\left[\mathbf{1} - \sum_{\mathbf{n,odd}}^{\infty} \frac{\mathbf{1}}{\mathbf{n^5}} \times \frac{\mathbf{192}}{\boldsymbol{\pi}^{\mathbf{5}}} \times \frac{\mathbf{h}}{\mathbf{w}} \mathbf{tanh}\left(\frac{\mathbf{n\pi w}}{\mathbf{2h}}\right)\right]^{\mathbf{-1}} \qquad \text{Equation 2}$$

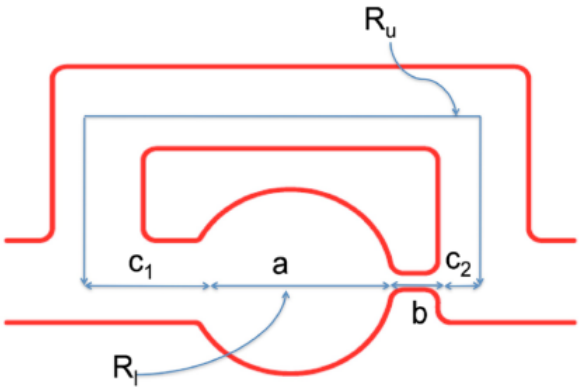

Figure 3. A sketch of the loop. [49]

Table 1. Design calculation for trap dia.=385µm**.** The resistances are calculated using Equation 1 and 2.

Trap Size cir385

		in meter	Micron
h		0.00008	80
wa		0.000385	385
wb		0.00005	50
wc1		0.0002	200
w2		0.0002	200
La		0.000385	385
Lb		0.0001	100
Lc1		0.0001	100
L2		0.00195	1950

µ(mineral oil)	0.03	Pa.s

n	fc2	fa	fb	fc1
1	0.250769	0.13037097	0.756729	0.250769
3	0.001033	0.00053651	0.004108	0.001033
5	8.03E-05	4.1719E-05	0.000321	8.03E-05
7	1.49E-05	7.7569E-06	5.97E-05	1.49E-05
9	4.25E-06	2.2078E-06	1.7E-05	4.25E-06
11	1.56E-06	8.095E-07	6.23E-06	1.56E-06
13	6.76E-07	3.5113E-07	2.7E-06	6.76E-07
15	3.3E-07	1.7168E-07	1.32E-06	3.3E-07
17	1.77E-07	9.182E-08	7.07E-07	1.77E-07
19	1.01E-07	5.2652E-08	4.05E-07	1.01E-07
21	6.14E-08	3.1922E-08	2.46E-07	6.14E-08
23	3.9E-08	2.0255E-08	1.56E-07	3.9E-08
25	2.57E-08	1.335E-08	1.03E-07	2.57E-08
27	1.75E-08	9.0858E-09	7E-08	1.75E-08
29	1.22E-08	6.3561E-09	4.89E-08	1.22E-08
31	8.77E-09	4.5538E-09	3.51E-08	8.77E-09
33	6.41E-09	3.3313E-09	2.57E-08	6.41E-09
35	4.78E-09	2.4822E-09	1.91E-08	4.78E-09
37	3.62E-09	1.8801E-09	1.45E-08	3.62E-09
39	2.78E-09	1.445E-09	1.11E-08	2.78E-09
Sum	0.251905	0.13096073	0.761247	0.251905

	Pa.s/m3
Ru	9.16E+12
Ra	8.09E+11
Rb	5.89E+12
Rc1	4.7E+11
Rl	7.17E+12

Rl/Ru	0.78231

Table 2. Design calculation for trap dia.=400µm**.** The resistances are calculated using Equation 1 and 2.

Trap Size cir400

		Micron
h	0.00008	80
wa	0.0004	400
wb	0.00005	50
wc1	0.0002	200
w2	0.0002	200
La	0.0004	400
Lb	0.0001	100
Lc1	0.0001	100
L2	0.00195	1950

µ(mineral oil)	0.03	Pa.s

n	fc2	fa	fb	fc1
1	0.250769	0.125482	0.756729	0.250769
3	0.001033	0.000516	0.004108	0.001033
5	8.03E-05	4.02E-05	0.000321	8.03E-05
7	1.49E-05	7.47E-06	5.97E-05	1.49E-05
9	4.25E-06	2.13E-06	1.7E-05	4.25E-06
11	1.56E-06	7.79E-07	6.23E-06	1.56E-06
13	6.76E-07	3.38E-07	2.7E-06	6.76E-07
15	3.3E-07	1.65E-07	1.32E-06	3.3E-07
17	1.77E-07	8.84E-08	7.07E-07	1.77E-07
19	1.01E-07	5.07E-08	4.05E-07	1.01E-07
21	6.14E-08	3.07E-08	2.46E-07	6.14E-08
23	3.9E-08	1.95E-08	1.56E-07	3.9E-08
25	2.57E-08	1.28E-08	1.03E-07	2.57E-08
27	1.75E-08	8.75E-09	7E-08	1.75E-08
29	1.22E-08	6.12E-09	4.89E-08	1.22E-08
31	8.77E-09	4.38E-09	3.51E-08	8.77E-09
33	6.41E-09	3.21E-09	2.57E-08	6.41E-09
35	4.78E-09	2.39E-09	1.91E-08	4.78E-09
37	3.62E-09	1.81E-09	1.45E-08	3.62E-09
39	2.78E-09	1.39E-09	1.11E-08	2.78E-09
Sum	0.251905	0.12605	0.761247	0.251905

	Pa.s/m3
Ru	9.16E+12
Ra	8.05E+11
Rb	5.89E+12
Rc1	4.7E+11
Rl	7.16E+12

Rl/Ru	0.781814

3.2 Cell culture and cultivation

The yeast cells used in the experiments were FY2 and P1A2 (SM14) [13,50] were obtained from Dr. Katy Kao's laboratory at Texas A&M University, College Station and are shown in Table 3. The details about the construction of the strains can be obtained from Ref [13], [50] and [51].

Table 3. Organisms [51]

Organism	Strain	Genotype	Reference
S. cerevisiae	FY2 (GSY1136)	Matα, ura3-52, gal+ in S288c background, YBR209W::Act1p-GFP-Act1t-URA3	Kao and Sherlock , 2008 [50]
	P1A2/SM14	YLH2 mutant P1A2. Isolated hyper-producer from evolution experiment.	Reyes et al., 2014 [13]

3.2.1 Yeast cultivation

The cells were cultivated and incubated in complex media Yeast Extract Peptone Dextrose (YPD) and YNB media at the conditions reported in the Ref [51]. The composition of the YPD medium used was as follows: 10 g/L yeast extract (Yeast Extract (Yeast Extract granulade; Fischer Scientific), 20g/L peptone (Bacto™ Proteose

Peptone ; BD) and 20g/L Dextrose (D-(+)-Glucose Dextrose; Sigma-Aldrich). The recipe of the YNB medium used was as follows: 20 g/L dextrose, 5 g/L ammonium sulfate (Ammonium Sulfate, BDH Aristar) 1.7 g/L yeast nitrogen base without amino acids and ammonium sulfate (Yeast Nitrogen Base, Amresco). YPD was autoclaved at 121^0C and YNB was sterile filtered using 0.22μm filter. The agar plates used for the cultivation of cells had 2% agar (R-2A Agar; Sigma-Aldrich) concentration.

Single colonies were picked from agar plates and incubated in 40mL of the YPD medium in 250mL shake flask. The cells (both FY2 and P1A2) were grown for 10 hours to bring the cells to exponential growth phase. 300μL of FY2 and P1A2 culture was then suspended in 40mL of fresh YPD in a 50mL centrifuge tube and 40mL of fresh YNB in a 50mL centrifuge tube, respectively. These solutions were then used for the encapsulation experiments.

3.3 Droplet storage, generation and cell encapsulation

The concept of droplet generation is explained in the Ref [8], [49] and [52]. The same concept for droplet generation, storage and cell encapsulation is used. Briefly, a sufficiently long plug of yeast culture with oil phase (Light Mineral Oil; Sigma-Aldrich) as the carrier fluid was created by manipulating hydrostatic pressure by changing the position of vials up and down in Figure 4. This cell culture was used to create an array of thirty droplets encapsulating single and multiple cells. The oil contained 2% (w/v) surfactant (Span 80; Fluka Analytical) for droplet stabilization.

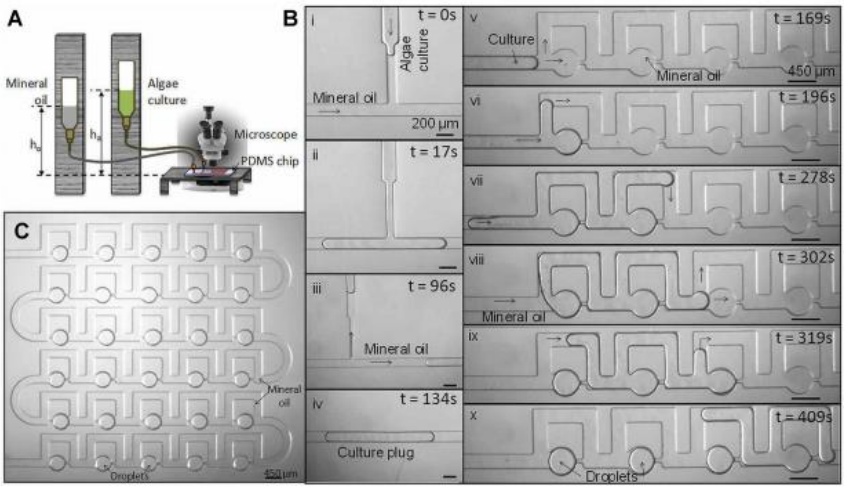

Figure 4. Droplet trapping using hydrostatic pressure for algal cells. Reproduced from Dewan et al [8]. The concept of trapping the yeast cells in the device is the same and in the figure yeast cultures are used instead of the algal cultures.

After generating the static array of droplets, the next challenge was to address the storage of the droplet. PDMS is diffusive to water and carbon dioxide, and though this advantageous for the gaseous exchange for the growth of the cells, it presents the challenge of droplet storage as the water from the droplet diffuses into the bulk. As a result, the droplet shrinks in size over time and the nutrient concentration changes over time. In the previous work [8], a scheme was proposed to overcome the challenge of droplet storage (Figure 5) and reported 30-day storage of the droplet without volume change. We used the same principle for our device with yeast cells. For more details, the reader is directed to Ref [8] and [49].

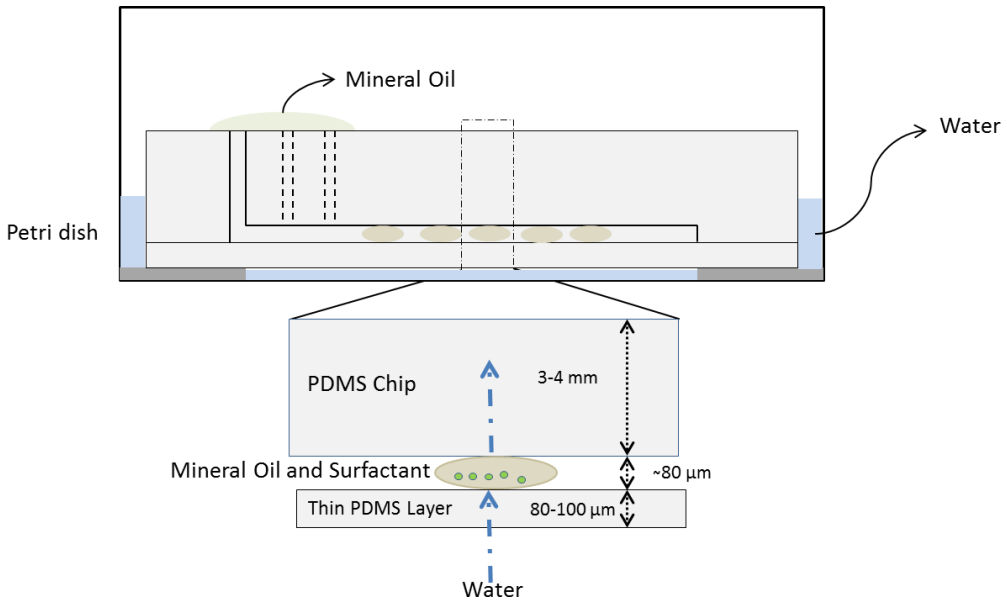

Figure 5. Long term storage of droplets (adapted from Dewan et al [8]). Yeast cells were observed Zeiss Axiovert 200M for over 50 hours.

3.4 Perfusion chip for algal cells

Our chip design was based on the perfusion chip proposed and tested by Rowat et al [53] for tracking the lineage of single yeast cells. Briefly, Rowat et al [53] designed the device to capture single *Saccharomyces cerevisiae* cells in a channel with constriction, and upon the capture the resistance of the main channel increases leading to flow diversion through the bypass channel. Guided by this work, our chip had a trapping channel with a constriction to trap the cell and a bypass channel. The device through continuous perfusion of media ensured that there was no nutrient depletion. This is unlike the case of constant volume droplet wherein the cell growth is limited by the availability of the nutrients. The device dimensions tested are reported in Figure 6. For additional details on device design and calculations the reader is directed to [53].

The details of cell culture and media composition for *Chlorella vulgaris* (UTEX 2714) are described in Ref [8] and [54]. 1 mL of algal cell culture was diluted in 40mL of media (final OD_{680}=0.0101) and was used to capture the cells into the device under a constant perfusion of media at flow rate of 30 nL/min. The chip was then observed under Zeiss Axiovert 200M and cell growth was observed for seven days at room temperature with cells subjected to 12h dark and light cycle.

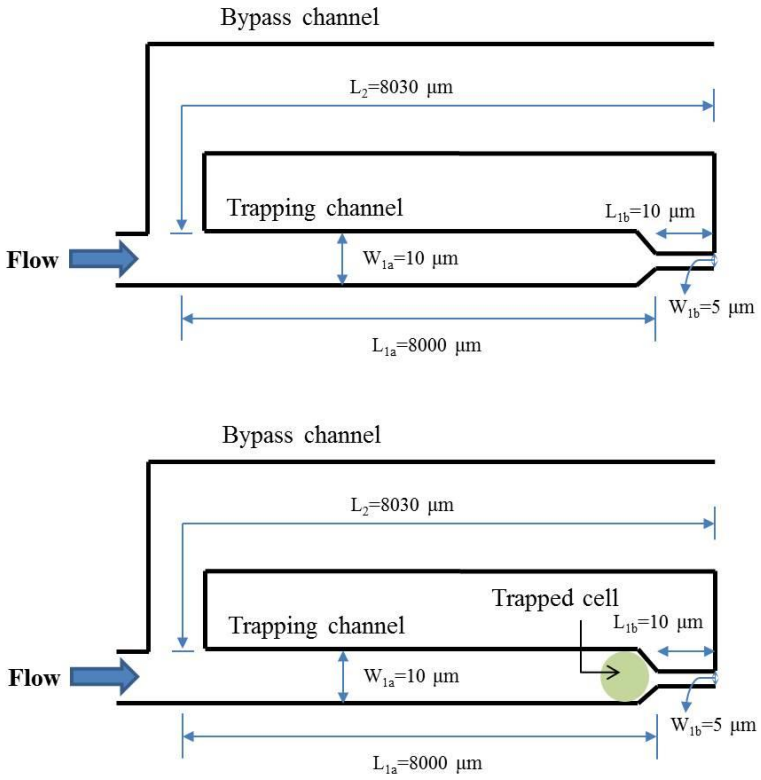

Figure 6. Dimensions of perfusion chip. The dimensions of the perfusion device tested are indicated in the figure. The resistance of the trapping channel increases upon capture of the flow cell. The cell is modeled as a solid incompressible sphere. The PDMS-device is fabricated using soft lithographic techniques.

The flow ratios modeled using a lumped element model are discussed in [53]:

$$\frac{\mathbf{Q_2}}{\mathbf{Q_1}} = \frac{\mathbf{R_{1a}+R_{1b}}}{\mathbf{R_2}} = \frac{\mathbf{h_2^3}}{\mathbf{l_2}}\left[\frac{\mathbf{l_{1a}}}{\mathbf{h_{1a}^3}} + \frac{\mathbf{l_{1b}}}{\mathbf{h_{1b}^3}}\right] \quad \text{Equation 3}$$

$$\frac{Q_2}{Q_1} = \frac{R_{1a}+R_{1b}+R_{1c}}{R_2} = \frac{h_2^3}{l_2}\left[\frac{l_{1a}}{h_{1a}^3} + \frac{l_{1b}}{h_{1b}^3} + \frac{l_{1c}}{h_{1c}^3}\right] \quad \text{Equation 4}$$

where Q is the channel flow rate and w, h, and l are the respective channel width, height, and length (subscript 1 and 2 refer to the trapping channel and bypass channel respectively). 1a, 1b and 1c refer to the straight length of the trapping channel, constriction and the cell respectively. Equation 3 describes the ratio of the flow rates without a cell in the trapping section and Equation 4 describes the ratio of the flow rates with a cell present in the trapping section. The cell dimensions of *Chlorella vulgaris* used for initial device design were as follows: l_{1c} =7 μm, w_{1c} =1 μm and h_{1c} =0.7 μm. Q_2/Q_1 = 4.28 without the cell and 13.8 with a single cell, for a device with $h=h_2=h_{1a}=h_{1b}$= 5 μm.

3.5 Design of membrane-less architecture for sub-micron separation

In this work the membrane-less filtration architecture for separation was patterned by flow of PK to etch portions of the substrate. As noted previously, the depth of the etched zone can be manipulated by varying the PK concentration, time and temperature. This technique was then used to fabricate a microfluidic architecture incorporating an embedded weir-like barrier. This architecture has two driving forces for

transportation of smaller-sized components across the barrier from inner lane to outer lane: curved flow path leads to dean vortices (secondary transverse motion) and unequal depths create a pressure gradient (and velocity gradient) across the barrier.

Curvature-induced forces (Dean vortices) permit the filtration barrier to be oriented parallel to the flow direction rather than perpendicular to it, thus avoiding clogging and minimizing the pressure drop. Dean number is described using Equation 5

$$\boldsymbol{\kappa = (\frac{D_h}{2R})^{0.5} Re}$$

Equation 5

where D_h =channel hydraulic diameter, R=flow path radius of curvature, and Re=Reynolds number. The dimensions used for the device design are reported in Figure 7 and Figure 8.

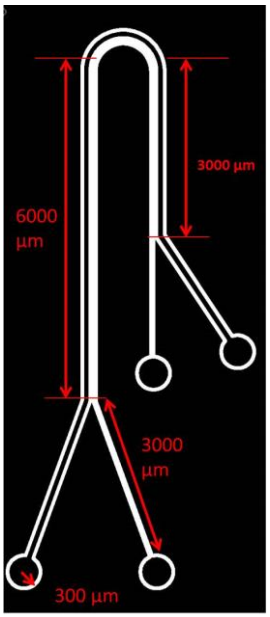

Figure 7. Top view of proposed device for sub-micron separation.

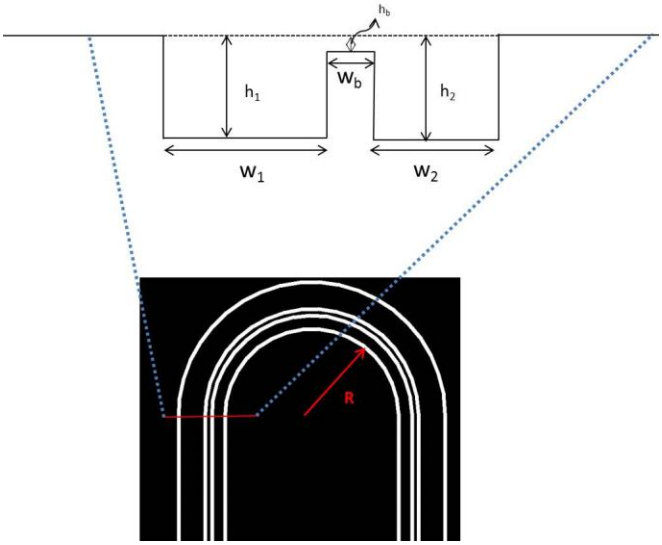

Figure 8. Sketch showing the dimensions of the channel. The dimensions marked are on the inlet side. h_1 = height of the channel-1 (i.e. outer channel in the figure), h_2 = height of the channel-2 (i.e. inner channel in the figure), h_b = height of the barrier (from base line) w_1 = width of the channel-1 (i.e. outer channel in the figure), w_2 = width of channel-2 (i.e. outer channel in the figure), w_b = width of the barrier.

According to CFD studies carried out using STAR-CCM+ by Dr. Aashish Priye (personal communication) it was found that the separation efficiency increases with the height difference. It was later realized that the separation is dependent more generally on the area ratio. This implies that the width change would also lead to separation for no height difference i.e. $h_1=h_2$.

4. FABRICATION

PDMS-based microfluidic devices were fabricated using standard soft lithography in the Cleanroom facilities of the Materials Characterization Facility (MCF) at Texas A&M University. The device designs were drawn in DWGeditor ™ 2009 (SolidWorks Corporation). The designs were used to print high-resolution (20,320 dpi) photolithography mask printed on transparency film from CAD/Art Services, Inc.

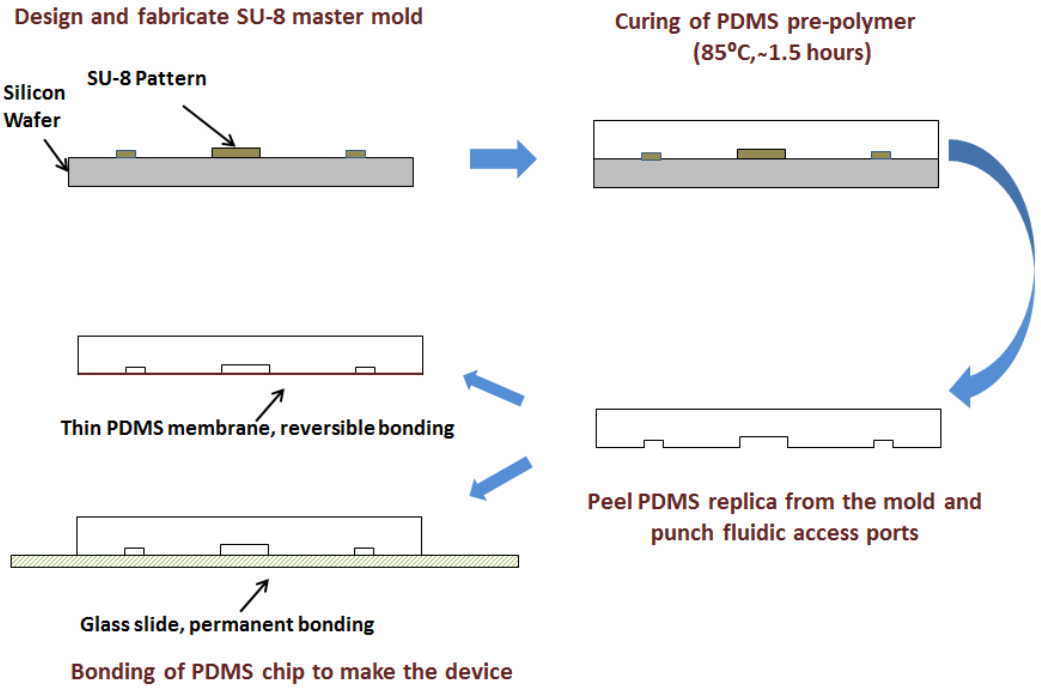

Figure 9. Steps involved in soft lithography**.**

Briefly, standard soft lithography comprises of the following basic steps: (1) spin coating of a photoresist onto the surface of thoroughly cleaned silicon wafers, (2) UV light exposure of photoresist through a mask (chrome/ transparency) for pattern generation, and (3) development of pattern by using developer solution to selectively

etch UV light exposed or unexposed regions. The resulting silicon wafer with the developed pattern is known as the master mold (Figure 9). This master mold, with a negative or positive imprint of the desired microchannel pattern, is used to cast a replica in the desired substrate material. PDMS was the desired substrate material because of its excellent optical, biocompatibility and gas permeability properties. The master mold is often given a silanization treatment for a prolonged usage of the mold and to facilitate the release of PDMS from the mold.

4.1 Fabrication of silicon master molds

Standard soft-lithography methods with a negative photoresist (SU-8 2050) were used to fabricate the SU-8 master mold in the Materials Characterization Facility. A high-resolution transparency film mask was used to obtain imprints of the microfluidic pattern on the silicon wafer substrate. These templates then served as negative molds to embed the desired inverse fluidic channels in poly (dimethyl) siloxane (PDMS, Sylgard 184, Dow Corning). A UV exposure of 21 seconds (Quintel Q4000 Mask Aligner**)** gave the best performing master mold.

4.1.1 Spin coating

Silicon wafers were rinsed using acetone (Fisher), 2-isoproponal (Fischer) and deionized water. The rinsed wafers are dried by using compressed air and placing on a hot plate at 200^0C for 10 minutes. SU-8 2050 (Microchem), a negative photoresist, is coated onto the surface of the wafer using a spin coater (Laurell WS-650S Spin Processor). A two-step process was used to achieve a uniform coating. The first step is

spinning at 500rpm for 10 seconds at an acceleration of 100rpm/s. The second step involves spinning at 2000rpm for 30 seconds at an acceleration of 300rpm/s. Photoresist coated wafer is soft baked by first heating at 65°C for 10minute, followed by 95^0C for 15minutes. The recommended time settings for different thicknesses can be found in SU8 Microchem manual. In our experience the recommended settings had to be adjusted significantly to obtain a stable master mold. The soft baked wafer is cooled down to room temperature (approximately after three hours) before proceeding with exposure step.

4.1.2 Exposure

The photoresist coated wafer is then exposed to UV light through a mask (using Quintel Q4000 Mask Aligner) to obtain imprints of the microfluidic pattern on the spin coated photoresist. Mask can be either a high resolution transparency or chrome mask. In our experience the high resolution transparency typically worked better for pattern dimension above 20 microns. Chrome mask worked better for resolving smaller dimensions. Various exposure settings over and under the recommended in the SU-8 Chem manual were tested to identify best exposure time for a given thickness was identified. A post exposure bake was done by heating the exposed wafer at 65^0C for 15 minutes, followed by additional heating of 95°C for 30 minutes. The wafer is then allowed to cool to room temperature. UV light exposure of the SU-8 photoresist results in evolution of nitrogen. We note the need to wait for 5-10 minutes after exposure to

complete the evolution process before setting the post exposure bake to get better master mold.

4.1.3 Development

The baked wafer from the previous step was developed using the SU-8 developer solution and dried. The SU-8 developer solution removed the unexposed regions of the photoresist. The developed wafer was hard baked at 200^{0}C for 10 minutes. This step ensured photoresist hardening and adhesion to wafer surface.

4.1.4 Silanization of the SU-8 mold

The mold were silanized with tridecafluoro-1, 2, 2, 2-tetrahydrooctyl-1-trichlorosilane (SIT8174.0, Gelest Inc.) to facilitate the ease of release of the PDMS from the master mold. Exposure of the SU-8 mold to the fluorosilane vapor is done in a desiccator attached to a vacuum source*;* a drop (20-µL) of fluorosilane is placed in a weighing boat in the center of the desiccator and vacuum is applied for one minute. The vacuum pump is removed and molds left inside the desiccator for at least 2 h at room temperature. The SU-8 master is then placed on a hot plate at 150°C for 10 minutes (to remove excess silane) and stored in a petri dish for future use.

4.1.5 Replica molding of PDMS from SU-8 master mold

The PDMS pre-polymer and cross-linker were mixed in a 10:1 wt. ratio and the mixture is degassed for 45 minutes. The SU-8 master is placed in a petri dish and the

PDMS mixture is poured on top of the SU-8 master. The petri dish containing the PDMS and the SU-8 master mold is heated at 80°C for 1.5 hours to cure the PDMS. The cured PDMS-covered SU-8 master mold is removed from the hotplate, and allowed to cool down, and the PDMS slab is gently peeled off from the SU-8 master mold. It is then rinsed with 2-proponal , and dried in a stream of compressed air to produce a soft elastomer template, and fluidic access ports, were punched using a 0.75mm biopsy punch.

4.2 Bonding the PDMS device to glass slide/PDMS thin layer

This PDMS chip is then bonded to another surface to create enclosed microchannels. This can be done in two ways: (1) permanent bonding to glass slide /cover slips using plama etcher, and (2) reversible bonding to a thin layer of PDMS.

4.2.1 Permanent bonding

Plasma etching (March Plasma Systems Model CS-1701) was used to create a permanent bond between PDMS chips and pre-cleaned glass slides/cover slips. The surfaces to be bonded are exposed to oxygen plasma in a plasma etcher (150 mTorr, 100 W, 40 s, oxygen gas flow rate of 10 sccm) [55-57] After exposure to plasma, the exposed surfaces are placed in contact with each other, and the composite is cured on a hotplate at 80°C for 10 minutes. The exposure to oxygen plasma makes the exposed surfaces hydrophilic. Overnight heating at 120°C restores the hydrophobicity of the PDMS, and the composite acts as hydrophobic [23,58].

4.2.2 Reversible bonding

The reversible bonding of the PDMS chip can be achieved by using PDMS prepolymer as a glue in two possible ways described as follows:

Stick and stamp technique [59]: PDMS chips were bonded reversibly to a glass slide using the transfer bonding technique with uncured PDMS as a glue/adhesive. 2-3 ml of freshly mixed degassed PDMS was poured on a glass slide, which was then spun at 8000 rpm for 8 minute in a spin coater. This resulted in a thin layer of uncured PDMS of thickness 1–1.5 μm on the glass slide. The previously fabricated PDMS chips are rinsed with isopropyl alcohol (IPA), dried using compressed air and by placing it on a hot plate at 80^0C to remove any solvent. This chip is then placed on the glass slide and lifted off, leaving a layer of uncured PDMS on it. Another glass slide is prepared for bonding by cleaning with IPA. PDMS chip with the thin layer of uncured PDMS was then placed on the glass slide and cured at 90°C for 15 minute to obtain the final device. The assembly was left at room temperature for 6 hours before use. Table 4 shows various spin coater settings resulting in different thicknesses of PDMS prepolymer on the glass slides.

Table 4. PDMS prepolymer as glue. Various settings were tested in the lab for thin PDMS layer on a glass slide.

PDMS thin layer on microscope glass slides				
	Steps	**Time (seconds)**	**RPM**	**Acceleration(RPM/s)**
A.	1	15	1500	200
	2	30	2500	300
B.	1	15	1500	200
	2	15	2000	300
C.	1	15	1000	200
	2	30	1500	300
D	1	8	8000	140
E	1	8-to-9 minutes	8000-9000	Not Available

PDMS Membrane at bottom of the device: PDMS chip containing the fluidic network was used as the top layer after peeling, punching the holes and cleaning with solvents. A thin membrane of PDMS was used as a bottom layer. The thin membrane was prepared by spin coating 2-3 mL of freshly mixed and degassed PDMS prepolymer on a silanized slicon wafer at 1,200 rpm for 30-60 seconds. The thickness of the bottom PDMS layer obtained ranged from 80 to 100 µm. Various settings were tested to obtain different thicknesses and reported in Table 5. This wafer was then placed on a hot plate at 65^0C for 15 minutes, and the top layer was gently placed and pressed. The assembly was heated at 65^0C for an hour and allowed to cool to room temperature. PDMS chip attached to thin PDMS membrane was then gently peeled off from the wafer.

Table 5. Thin Layer of PDMS on 3" diameter silicon wafer. This layer is used as a membrane for the PDMS chips.

	Step	RPM	Acceleration (RPM/s)	Time	Expected thickness (micron)
A.	1	2500	140	5 minutes	10
B.	1	500	100	30 sec	70-100
	2	1200	100	30 sec	
C.	1	8000	140	8min	~1-1.5
D.	1	1200	140	30 sec	~70-100

4.3 Perfusion chip for algal cells

PDMS-based devices were fabricated using SU8-2007 photoresist master mold (using a chrome mask in the exposure step) of height 8 micron fabricated as described in Section 4.1. This PDMS device was bonded to a cover slip by exposing both the cover slip and the PDMS device to oxygen plasma (Section 4.2.1).

4.4 PLA fabrication

4.4.1 Template for enzymatic etching

The etching templates were made using soft lithography method was described previously. Access ports were punched in the PDMS slab (peeled off from the master mold) using a 20 gauge blunt end stainless steel needle. The PDMS chip containing microchannels were rinsed with 2-propanol and dried in a stream of compressed air. The cleaned PDMS chip was directly adhered to a flat PLA substrate to produce enclosed

channels. Tygon tubing (0.03 inch OD; Small parts, Inc.) was inserted into the access ports and the PDMS was pressed firmly to ensure a tight seal between the microfluidic template and the PLA substrate. A good contact between PLA and PDMS was very critical as the contact was just physical and prone to leakage. Unevenness in the surfaces resulted in air pockets and there was leakage during enzymatic etching step, and hence the need of removing the pockets.

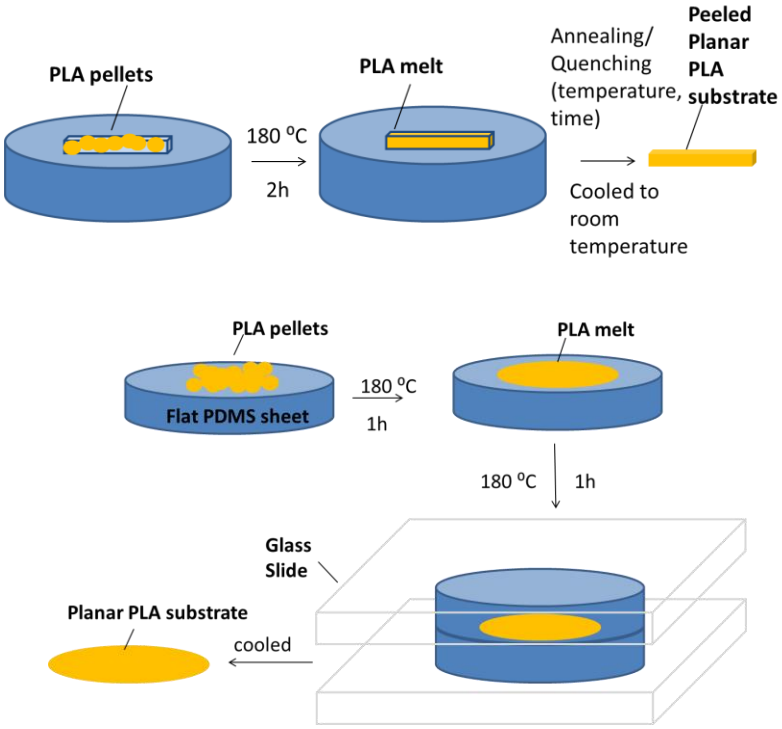

Figure 10. Steps involved in the fabrication of the planar PLA substrate.

Smooth planar PLA substrates were obtained by placing pelletized PLA resin (NatureWorks, grade 3052D; Jamplast Inc.) directly onto flat PDMS slab. The PDMS slab containing the PLA pellets was heated to 180 °C under vacuum for 1-2 h, followed

by an additional 1 h of heating after vacuum removal. The slides were then cooled at room temperature for 1 h, after which the PLA film could be easily peeled away (Figure 10).

4.4.2 Enzymatic etching

Solutions of PK (MW = 28.9 kDa; BP1700, Fisher Scientific) and BSA (MW = 66.4 kDa; A2153, Sigma-Aldrich) were prepared in Tris-HCl buffer (pH 8.0; BP1758, Fisher Scientific). 15 mL of 1M Tris-HCl buffer was diluted with 485 mL of DI water to obtain a buffer stock concentration of 30mM, which was used in all the experiments. 0.05 g of proteinase K was dissolved in 250 mL buffer to give an etchant concentration of 0.2 mg/mL (6.92 μM) used in all the experiments. 1% (w/v) BSA in the diluted buffer was used in the experiments. The solutions were stored at 4^0C and used as required.

The templates were cleaned by placing them in an ultrasonicator for 5 minutes, followed by thorough rinsing with DI water and 2-propanol, and cleaning with scotch tape before contact with the substrate. Syringes (3 mL; BD Plastic) with solutions were mounted on a syringe pump (PHD 2000; Harvard Apparatus) and the fluidic connections with the template-substrate assembly were checked for leakage. This entire setup was then placed inside an incubator while the etching solutions (enzyme, BSA, DI water, buffer) were continuously pumped though the network at 37°C. The enzyme solutions were changed every six hours to prevent enzyme degradation. Etching was also carried out at room temperature (74^0F=24.4^0C).

After completion of etching, the PDMS template was removed from the PLA substrate. To stop the enzymatic reaction the resulting patterns were washed using 2-propanol and DI water, and dried using compressed air. A profilometer (Dektak 3 stylus profilometer; Veeco Instruments) was used for depth measurements of the etched channels.

4.4.3 Membrane-less filtration device

The membrane-less filtration architecture for sub-micron particle etching was fabricated using the following procedure (Figure 11):

Microfluidic template 1 was first used to create channels of equal depth by the flow of enzyme proteinase-K to achieve a desired etch depth (Figure 11a and Figure 11b). This step was followed by changing one of the streams to the template 1 by DI water and keeping the other one to proteinase-K. No etching took place in the region with flow of DI water; however, continued flow of enzyme led to further etching on the other side, resulting in desired unequal depth separated by a barrier (Figure 11c). Next, etching template 2 was aligned over the etched portion, and etching of the region bounded by the template takes place. This region now includes previously etched region as well as un-etched barrier (Figure 11d). The final channel geometry is shown Figure 11e.

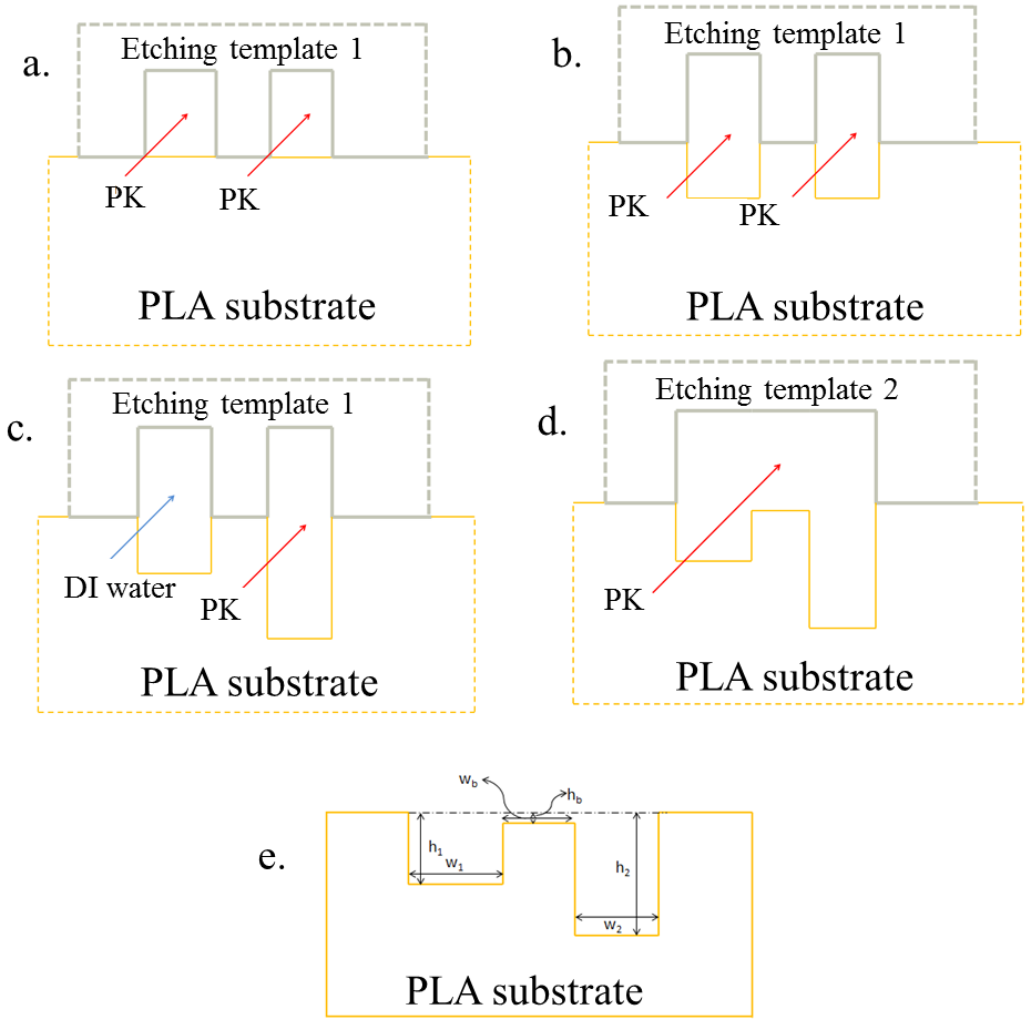

Figure 11. Flow scheme to etch PLA without enzyme inhibitor. In a. and b, etching of PLA substrate takes place by flow of enzyme PK in both the channels of template1. In subsequent step c, enzyme flow is replaced by DI water on one side resulting in no etching in that channel and continued in etching in the channel with flow of PK. In last step d, etching template 2 is used to etch the entire PLA surface under the template to ultimately yield the desired dimensions on the substrate (e).

This etched PLA template was replicated into PDMS by adding a 10:1 degassed mixture of the PDMS elastomer and curing agent to the template on a hot plate at 50°C for 5 hours. PLA has a glass transition temperature of 60-65°C [9] and etched PLA substrate with PDMS mixture is heated at 50°C to avoid deforming the pattern on PLA. The PLA template left an inverse replica of itself in the PDMS. This replicated feature in PDMS is referred to 'Replicated PDMS template' or 'PDMS replica' in Figure 12. This PDMS replica then served as a master mold to replicate the etched substrate. This replication process from provided a convenient starting point to obtain final etched PLA substrate instead of carrying out enzymatic etching multiple times.

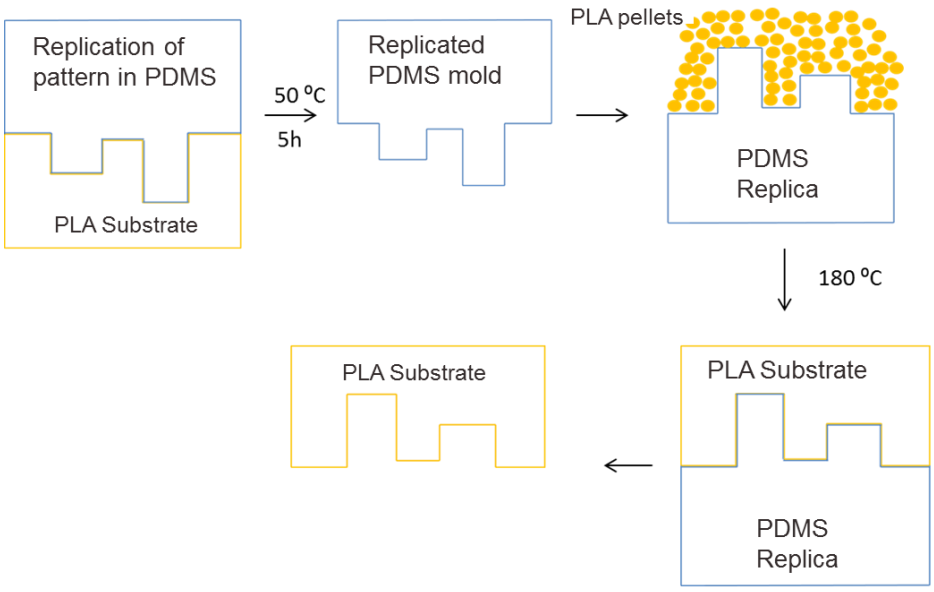

Figure 12. Replica molding. The figure above shows the steps involved in replicating the etched pattern from PLA substrate. An etched pattern is first replicated into a PDMS mold, and PLA pellets are melted and subsequently solidified on this PDMS replica to generate microchannel geometry in PLA substrate without the need for enzymatic etching each time.

Before bonding, the fluidic access ports were drilled into PLA substrate with micro-channels using a drill bit. The substrate was thoroughly rinsed with 2-propaol and ultrapure water, and dried using compressed air. The scanning electron microscope (SEM) images of enzymatically etched channel with and without the drilled access port are shown in Figure 13. Alternatively, PDMS pillars as shown in Figure 14, described by Huang et al [9], could be used to access fluidic ports.

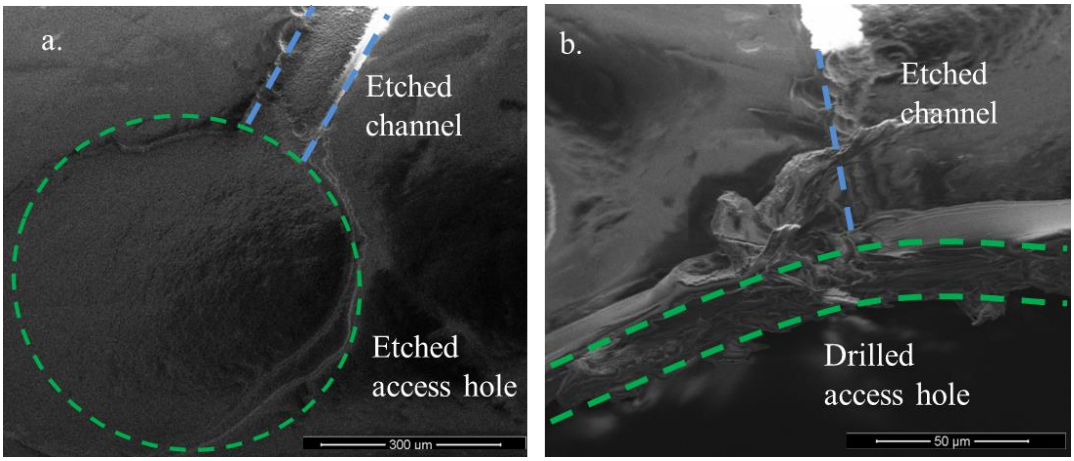

Figure 13. Scanning electron microscope images of the etched channel. a. represents image of enzymatically etched channel where an access hole has not been drilled; b. represents the image of an etched channel with the access hole drilled.

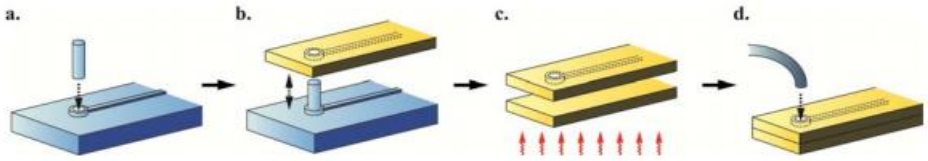

Figure 14. PDMS pillars to create fluidic access ports [9].

This substrate was then bonded to a flat piece of PLA by thermal treatment. The flat piece of PLA was placed in contact with the etched substrate using a vacuum sealing apparatus, commercially used to vacuum package food (as shown in Figure 15a). The vacuum sealed bag was then placed in a vacuum oven (maintained at 60^0C) for 30 minutes for thermal bonding (Figure 15b). Vacuum packing ensured a gentle and uniform pressing of the device to ensure proper contact and bonding.

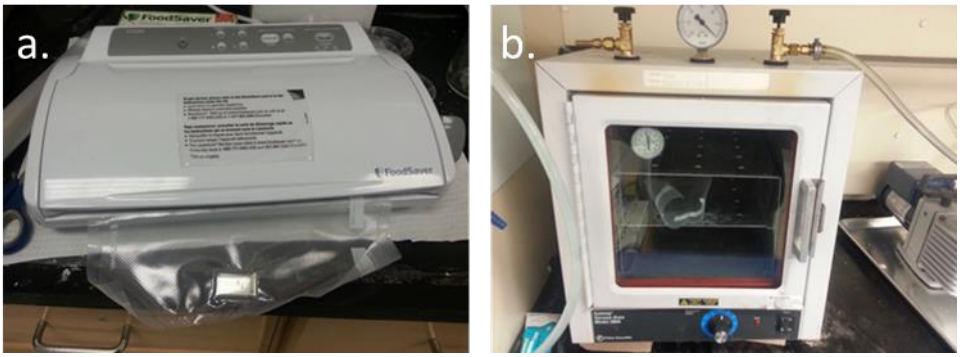

Figure 15. Thermal bonding of etched PLA to flat piece of PLA. a. Etched PLA and flat piece of PLA being sealed by a vacuum sealer for gentle and uniform pressure on the assembly b. The vacuum sealed bag placed in the oven for heat treatment.

Tygon tubing (0.03 inch O.D.) was inserted into the fluidic access ports and sealed using epoxy glue. Aqueous solutions of dyes (or aqueous particle/cell solutions) were used on the inner channel, while the ultrapure water (or buffer) was infused from the outer channel.

PLA pellets were melted in an oven maintained at 180°C, and then treated the following two ways: i. cooled to room temperature (25 °C) by removing it from 180°C oven to room temperature (referred as substrate A from hereafter); ii. cooled to 0°C by

removing it from 180°C by placing the PDMS mold containing PLA on block of ice (referred as substrate B hereafter). The way molten PLA pellets are solidified by cooling results in different crystallinity of the final substrate [9].

5. RESULTS AND DISCUSSION

5.1 Droplet experiments

The droplet storage technique from Dewan et al [8] was successfully employed to monitor the growth of yeast cells in the droplets for a period of 48 hours (Figure 16). Additionally, we were successfully able to encapsulate single and multiple yeast cells in the in the static droplet array.

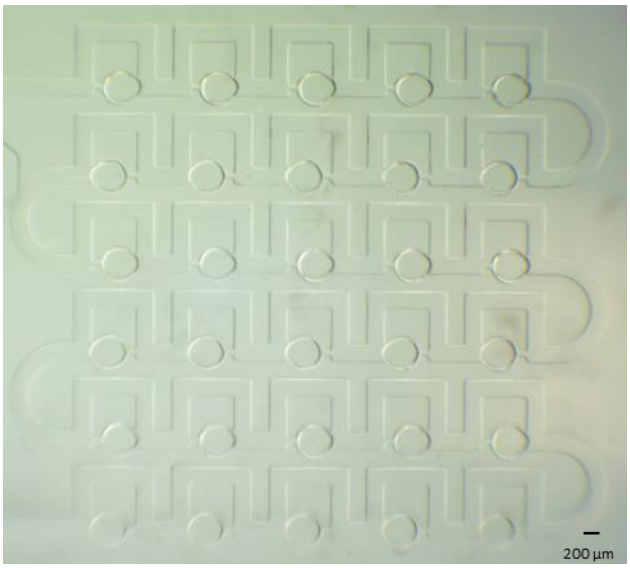

Figure 16. Static droplet array of YPD media. The droplets of the media are surrounded by the oil phase (Mineral oil mixed with Span 80 surfactant).

The results from one such encapsulation experiment are reported in the Table 6 and Figure 17. In the experiment, 41 cells were encapsulated in 22 droplets, thus giving an average number of cells per drop of 1.86. The cells encapsulation in the droplets was

compared to Poisson distribution for trapping the cells. Poisson distribution (the probability of random encapsulation of cells) is given by the following equation:

$$\mathbf{f(k,\lambda)} = \frac{\boldsymbol{\lambda^k e^{-\lambda}}}{\mathbf{k!}} \qquad \text{Equation 6}$$

where, f = probability of encapsulating, k = number of cells in the droplets, and λ = average number of cells in the droplets.

Table 6. Encapsulation statistics.

Number of cells	Number of droplets	Observed probability of encapsulation	Poisson distribution of encapsulation
0	2	0.091	0.155
1	8	0.364	0.289
2	7	0.318	0.269
3	3	0.136	0.167
4	1	0.045	0.078
5	0	0.000	0.029
6	1	0.045	0.009

Figure 17 depicts a graphical comparison between the encapsulation from the experiment and random encapsulation (Poisson distribution). For this particular experiment (λ=1.86) Poisson distribution predicted a higher number of empty droplets (k=0). This experiment also resulted in a higher encapsulation efficiency of single (k=1) and double (k=2) cells compared to the predicted random encapsulation efficiency. However, the efficiency for encapsulation of three (k=3) and four (k=4) cells in the experiment was lower than random encapsulation value. There was no droplet with five

cells and the fraction of droplets with six cells is much higher than a random encapsulation.

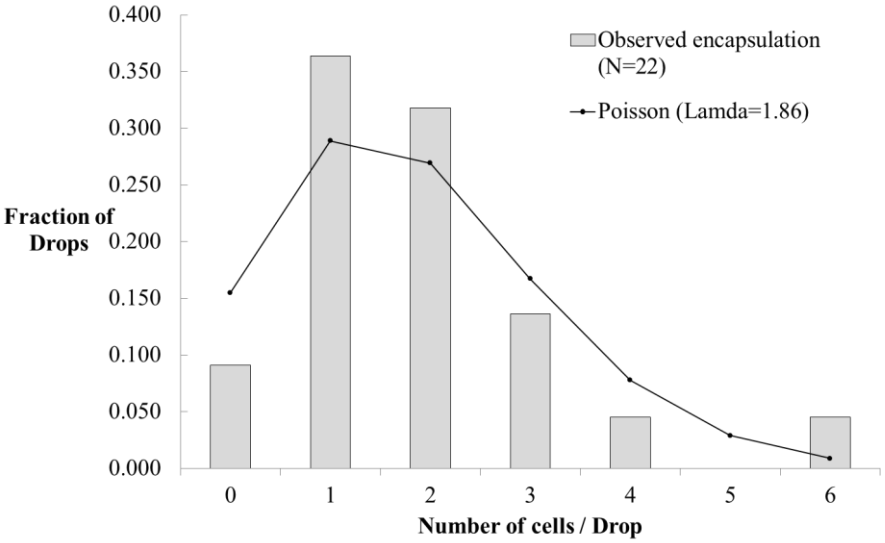

Figure 17. Observed encapsulation efficiency and Poisson distribution. The figure shows a comparison of the fraction of drops for a given number of cells per drop for the observed encapsulation with the Poisson distribution.

Clearly, this experiment has significant deviations from Poisson distribution. A deviation from the random encapsulation is indicative of biases (and perhaps potential flaws) in the experimental setup. Cell settling in the syringe and tubing at the time of generation of the plug to create the static droplet array would lead to deviations from the random encapsulation. A feasible solution to overcome this challenge would require buoyancy matching the cells with cells. Chemicals like OptiPrep [23] (Sigma-Aldrich) can be added for buoyancy match but the impact of such compounds on cell physiology must be clearly established beforehand. Furthermore, more experiments need to be

conducted to increase the sample size (N=22) and could possibly remove the deviation from random encapsulation.

The controlled encapsulation of single and multiple cells in a droplet is efficiently represented in Figure 18 (adapted from Ref [23]). This Venn diagram represents that the rate of droplet generation, flow rates determining the shear stress and pressure experience by the cell (cell viability) and cell ordering for capturing the desired number of cells represents the regime where controlled encapsulation occurs. A different experimental design for reference [23] enabled a cell encapsulation in kilohertz (kHz) frequency. However, our work used a different mechanism (T-section) for droplet generation and hence different results. With our technique, we were able to generate the drop and create as static droplet array simultaneously. Moreover, reference [23] used beads as cell surrogates and thus were able to go to achieve higher flowrates (and encapsulation).

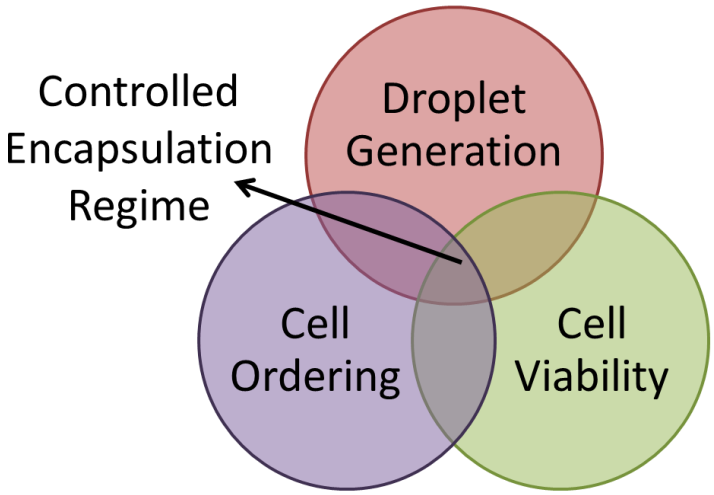

Figure 18. Controlled encapsulation regime**.** Venn diagram representing the controlled encapsulation regime as the intersection of droplet generation, cell ordering and cell viability [23].

Once the single and desired multiple cells were encapsulated in the static droplet array time-lapse brightfield microscopy could be used to monitor the growth of the cells as shown in Figure 19.

Kinetic parameters like specific growth rate, μ, can be calculated using equation 4, where the cell count was established using microscope images in the droplet over time (using ImageJ software).

$$\boldsymbol{\mu = \frac{d\ln(N)}{dt}} \qquad \text{Equation 7}$$

where, N= number of cells, and t=time.

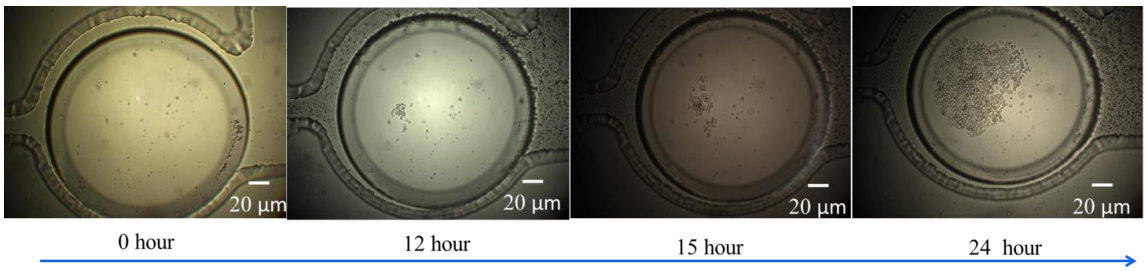

Figure 19. Single yeast cell in YPD droplet at different time of observation. Microscopic images of a droplet at different times with a single yeast cell (FY2 in YPD media) at the beginning of the encapsulation process.

In Figure 20 and Figure 21, the numbers of yeast cells (FY2 and P1A2) were plotted against the time for different initial cell concentration and cell media (YNB and YPD). The specific growth rates for the FY2 cells in YPD media were: 0.26 h^{-1} for droplet #34 (initial cell=3), 0.21 h^{-1} for droplet #44 (initial cell=3) and 0.30 h^{-1} for

droplet #24 (initial cell=1) respectively. The specific growth rates for the P1A2 cells in YNB media were: 0.25 h^{-1} for droplet #12 (initial cell=2), 0.21 h^{-1} for droplet #11 (initial cell=2) and 0.23 h^{-1} for droplet #31(initial cell=1) respectively. The cells reach a stationary phase at roughly around 24 hours, and densely packed colony of yeast cell in the droplet could be observed. The stationary phase corresponds to the point when the droplet is exhausted of the nutrients to support biomass growth. The growth of the cells in the droplet corresponds to the growth of cell in batch bioreactor, with no mixing.

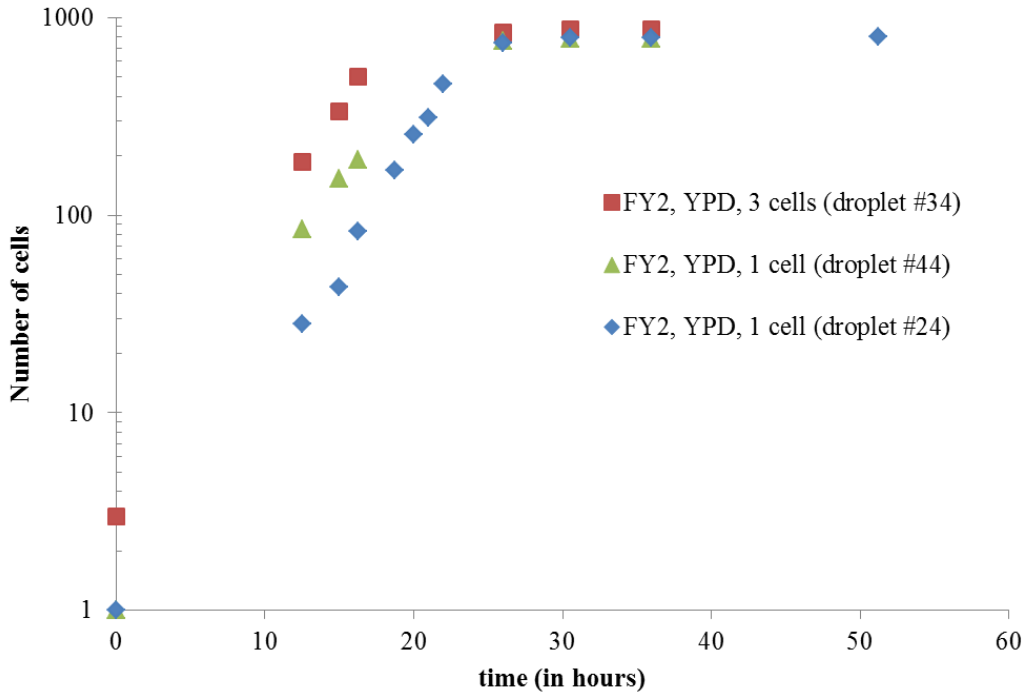

Figure 20. Growth curve of *Saccharomyces cerevisiae* (FY2) in YPD media droplet at room temperature (25 °C). Red, blue and green curve represent a starting cell count 3, 1 and 1 cell respectively. Droplet # indicates the location of the droplet on array.

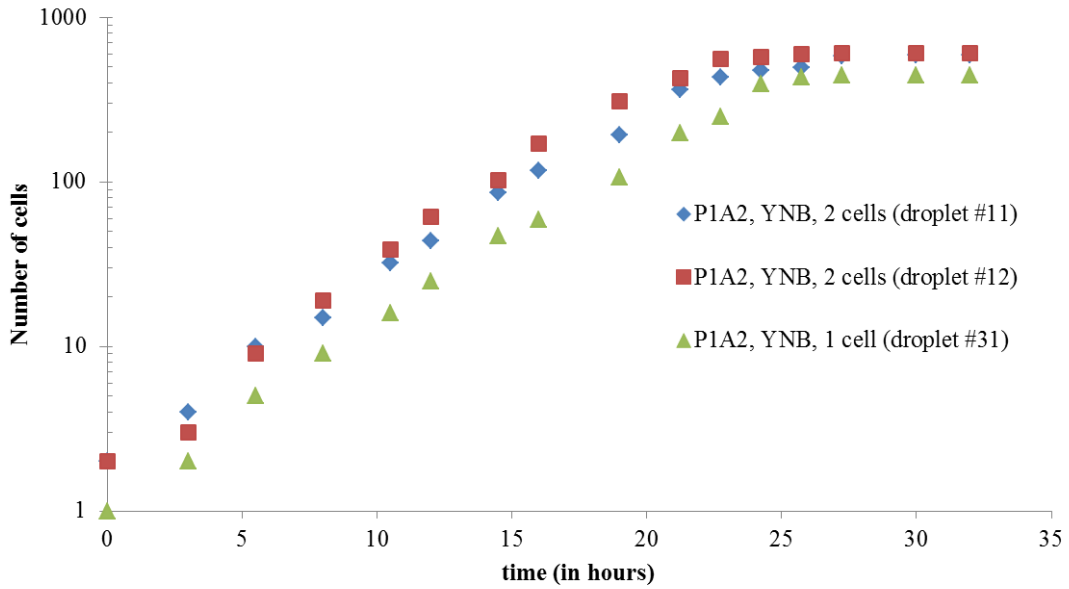

Figure 21. Growth curve of *Saccharomyces cerevisiae* (P1A2) in YNB-media droplet at room temperature (25 °C). Red, blue and green curve represent a starting cell count 2, 2 and 1 cell respectively. Droplet # indicates the location of the droplet on array.

The heterogeneities in *S. cerevisiae* were not as significant as growth heterogeneity noted in the case of algal cells by Dewan et al [8]. Heterogeneity in growth rate arises from heterogeneous cell division of the *C. vulgaris* autosporangium (refer to Section 2.2). Yeast cells, however, divides using binary fission and thus does not give significant heterogeneity. The heterogeneity in the growth rates of the yeast cells in our preliminary data could shed some light into the physiological response of the cell to the genetic modification and media composition. Additional experiments would be required to establish how the single and multiple cell encapsulated cells impacted the growth rate under different media conditions. The variations can be noted clearly from

Figure 20 and Figure 21; however, more data needs to be collected to obtain conclusive results.

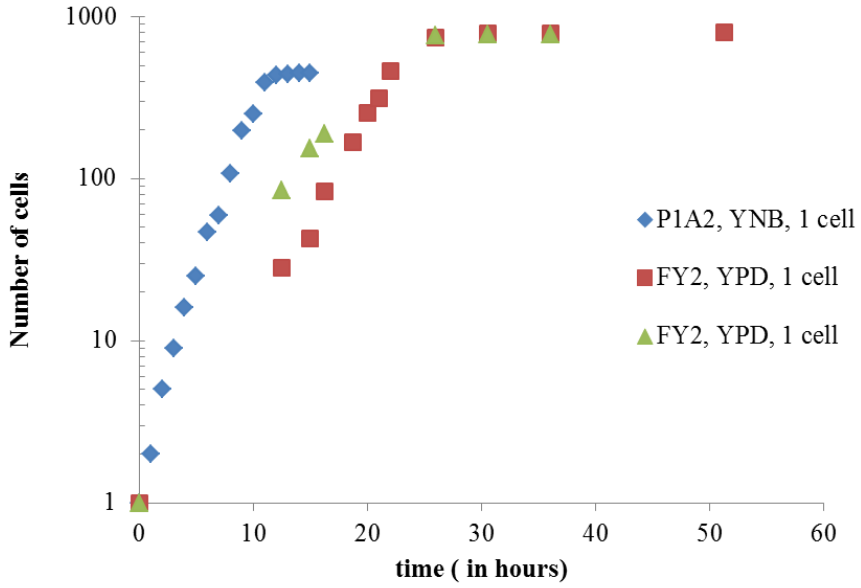

Figure 22. Growth curve of single cells. Growth curve of *Saccharomyces cerevisiae* single cells of FY2 and P1A2 in YPD and YNB media from Figure 20 and Figure 21 at room temperature (25 °C).

The comparison of the growth rate of the cells (starting with a single cell) is reported in the Figure 22 and the specific growth rates are reported in Table 7. The single cell (P1A2) in YNB droplet grew much faster than the single cells of FY2 in YPD droplet, and reached a stationary phase around ~10hours. The single cells of FY2 in YPD droplet reached a stationary phase in approximately ~ 24 hours. This difference in time required to reach the steady state is possibly due to the genetic difference between the cells coupled with the difference in the media composition. It is also possible that the

cells at the time of encapsulation were in different cycle of cell division. This would imply that the single cell captured in the YNB droplet was more active and required shorter time to reach the steady state. The cells in both the cases were cultivated from the exponential phase of the shake flask (after 10 hours of growth in ~50mL YPD in an incubator); however, the growth of the individual cells within the macroscopic volume could possibly be in any stage of the growth phase. Cell synchronization studies could be conducted to eliminate or/and understand the differences in growth rate.

Table 7. Growth rate data.

Droplet #	Strain	Media	N_0	N_f	μ (hr^{-1})
11	P1A2	YNB	2	590	0.23
12	P1A2	YNB	2	608	0.25
31	P1A2	YNB	1	445	0.23
34	FY2	YPD	3	867	0.26
44	FY2	YPD	1	781	0.21
24	FY2	YPD	1	800	0.303

It is worth noting that in unpublished work to model the growth of yeast cells (SM14 in YNB) in bioreactor and shake flasks studied under optimal operating conditions [51], a maximum specific growth rate of 0.251 hr^{-1} has been obtained. Thus,

the specific growth rate of the SM14 in our droplet is comparable to that obtained by bulk culturing techniques.

5.2 Perfusion chip for algal cells

The cells were captured in the perfusion chip as described in Section 3.2. Growth of trapped cells was observed using an inverted microscope Zeiss Axiovert 200M and preliminary observations are reported here. Observations of one such trapping channel with multiple cells is shown in Figure 23. The number of cells captured in this channel at the start of the experiment was 5. The cells were imaged under an inverted micrscope after t=24 h, t=36 h, t=48 h, t=60 h, t=72 h, t=96 h, t= 144 h, t= 156 h and t=168 h respectively. After 24 hours of capture, none of the cells had started dividing. At t=36 hours, three cells started to divide and continued growing for the rest of the experiment and the remaining two cells started dividing after 48 hours. Monitoring of the individual daughter cells was limited by the 20X objective magnification lens and crowding of the cells. In our preliminary study, the cells were monitored at 12-24 hour intervals, as also indicated in Figure 23. An approximate and quantitative growth rate could be obtained if the cells were observed at shorter intervals of time.

Additionally, we captured a single cell, shown in Figure 24. This cell grew very slowly over a period of 6 days and appeared to be still undergoing its first cell division at end of 144 hours (6^{th} day).

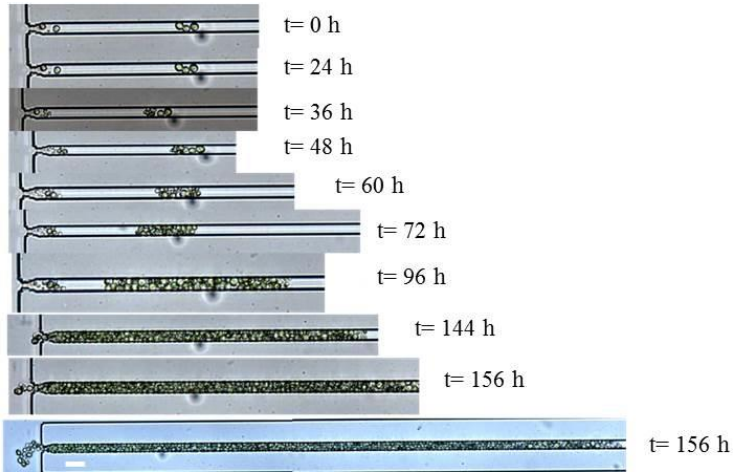

Figure 23. Time evolution of growth in a cluster of five algal cells at room temperature in the perfusion device. The image at t=0 h correponds to the five cells captured in the device at the beginning of the experiment. The cells were imaged under an inverted micrscope after t=24 h, t=36 h, t=48 h, t=60 h, t=72 h, t=96 h, t= 144 h, t= 156 h and t=168 h respectively. The white bar in the bottom micrograph corresponds to a length of 10 microns.

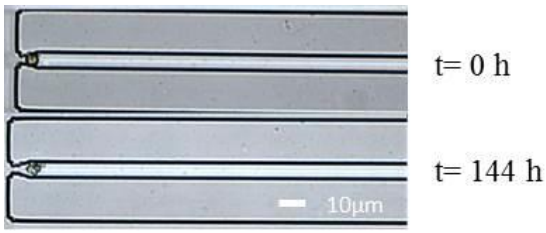

Figure 24. Time evolution of single algal cell in the perfusion chip. Microscope images were obtained at t=0 h and t=144 h. The scale is shown in the figure.

Cell growth in both the above cases indicated a slow initial growth (i.e. the number of cells increased slowly), consistent with the trends observed by Dewan et al for single cells in their droplet-based study. This is indicative of the inherent slow growth of *C. vulgaris* cells represented by a long lag phase. Additionally, during the

exponential growth phase where the cells divide rapidly, the daughter cells were much smaller in size compared to the mother cells. This correlated with the size distribution observed by [8] where the cell size decreased during the exponential growth phase in a droplet.

5.3 Enzymatic etching

Fabrication and enzymatic etching of substrate A and B were carried out as reported in Section 4.3. A scanning electron microscope image of an enzymatically etched channel is shown in Figure 25.

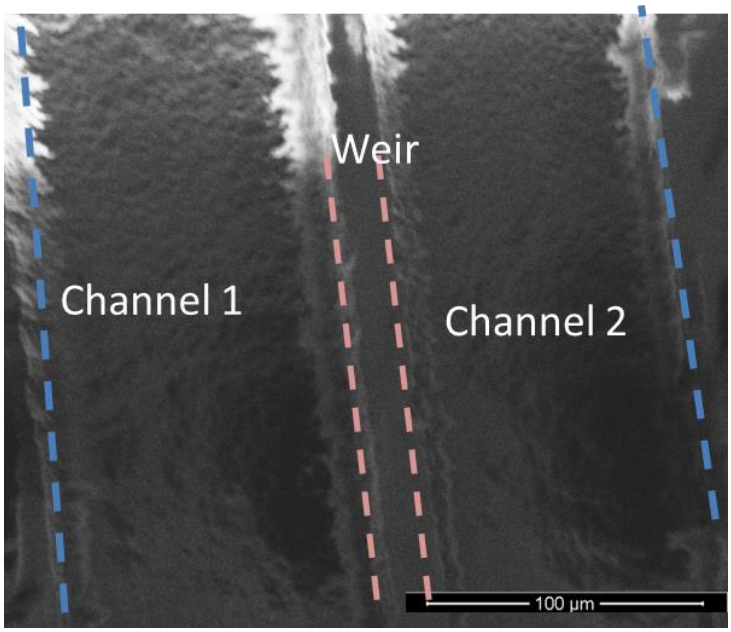

Figure 25. Scanning electron microscope image of enzymatically etched PLA. The weir is shown in dotted light red lines and the edges of the channels are shown by dotted blue line.

Figure 26 represents the plot of variation of the etch depth with time for substrates A and B at two different temperatures (24.4^0C and 37^0C). An enzyme concentration of 6.92 μM was used for the experiments based on data reported by Huang et al [9]. A flow rate of 0.5 μL /min was used for these experiments. A given value plotted in the graph is average of four etch depths obtained per etching experiment. Two etch depths were obtained at the inlet and two etch depths were obtained at the outlet. The error bars in the plot represent the standard deviation of the four etch depths from the mean value.

Figure 26 represents a linear variation of the etch depth with time for both substrate A and B at both 24.4^0C and 37^0C. Characteristic etch rates of 1.45 μm/h and 0.16 μm/h were obtained for substrate A at 37^0C and 24.4^0C respectively. For substrate B, characteristic etching rates of 1.28 μm/h and 0.16 μm/h were obtained at 37^0C and 24.4^0C respectively (refer to Table 8).

The variation of the etch rate with temperature for substrate A and B was noted from the graph and corresponded to an increased enzymatic etching at higher temperature. These results followed the trend observed by Huang et al [9] in their work. Moreover, substrate A and B had approximately the same behavior at both the temperatures, which suggested that the cooling of the substrate to prepare the final substrate did not influence the etch depth.

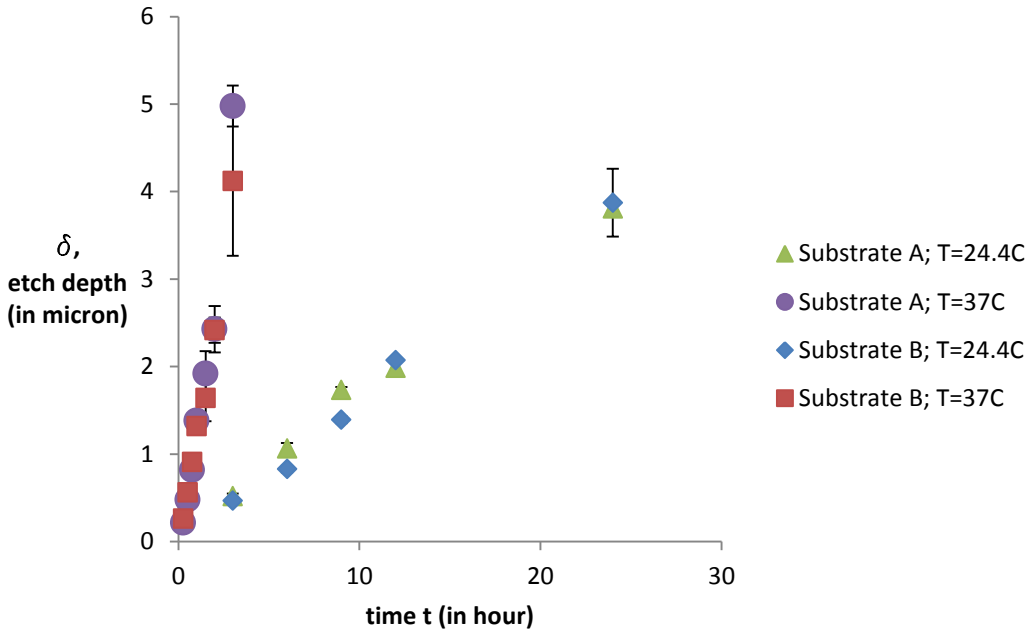

Figure 26. Plot of etch depth against time. The plot represents the variation of the depth of PLA etched (in microns) with time (hours) for Material A and B at temperatures of 24.4^{0}C and 37^{0}C. A flow rate of 0.5 µL/min and enzyme concentration of 6.92 µM was used for all the experiments. The values in the graph represent an average value for four etch depths (two at the outlet and two at the inlet of the geometry) and the error bars represent the standard deviation of the readings from the mean value.

Table 8. Characteristic etch rate of the PLA substrate at 24.4°C and 37°C. The minimum depth for the two substrates is also reported for t=3 hour, T=24.4°C and flow rate of the enzyme=0.5 µL/min.

Substrate	**Etch rate at 24.4°C**	**Etch rate at 37°C**	**Minimum depth measured (at 24.4°C)**
A	0.16 µm/h	1.48 µm/h	~51 nm
B	0.16 µm/h	1.25 µm/h	~ 46 nm

The error bars in Figure 26 were indicative of the variation of the four measured etch depths for a given condition for a given substrate. The slight variation most likely resulted from the degradation of the enzyme in solution or fluctuation of the temperature. The etching solution of PK used in the experiment was created in bulk volume of 250 mL and stored in the 4^0C refrigerator. 6-mL (two 3-mL syringes) were used for a single experiment and drawn from the stock. The delay in the use of the enzyme could potentially change its activity as some of the enzyme degraded and resulted in the noted variation in the etch depth. The experiment at 24.4^0C was carried out at room temperature and a fluctuation of the room temperature could have also caused the observed variations in the depth. For a more reliable data corresponding to 24.4^0C, the assembly should ideally be placed in an incubator.

The outer channel has a depth of ~8 μm and the inner channel is of ~8 μm. The cross sections obtained were not rectangular as idealized in Figure 5 but rather trapezoidal. For simulation purposes the cross section can be assumed to be rectangular. The depths of the channel varies linearly with time and different etch rates are obtained at different temperatures as expected

Moreover, we observed a difference between the etch rate of the original study [9] and the current study. Huang et al [9] reported a characteristic etch rate of 2μm h^{-1} at 37^0C and enzyme concentration of 6.92μM and flow rate of 5 μL min^{-1} . The PLA resin used for the work was Natureworks grade 3051 D (Jamplast Inc.). The PLA resin used for this work was Natureworks grade 3052D and this leads to the difference in etching rate.

The minimum depth for an etching experiment at 37^0C resulted in etch of ~215 nm on substrate A and ~260nm on substrate B (time=15min). And the minimum depth etched at 24.4^0C on substrate A and B was ~51-nm and ~46-nm, respectively (t=3 hours). The smaller etch depth over longer time showed an enhanced control on features dimension for lower temperature value. Similarly, a deeper depth in shorter period could be used by etching at a higher temperature. Thus, it took much longer for an enzyme to etch a depth at room temperature to etch a given depth but it gave much better control over the etch depth.

Once the etch rates were obtained, the enzymatic etching process was used to fabricate the desired architecture for separation. The final geometry was obtained the in this fashion by carrying out the enzymatic etching for 4 hours at room temp and 8 hours at 37^0C. The enzyme solutions were changed every 6 hours to avoid the degradation of the enzyme and hence the variation of etch rate. Replica molding was used to replicate the etched mold.

Additionally, a barrier height of ~500nm, i.e. h_b~0.5μm, created in this fashion provides the basis for a proposed biodegradable device for separation of the exosomes and larger sub-cellular components from the inner channel.

6. RECOMMENDATIONS AND FUTURE WORK

6.1 Static droplet array

Our microfluidic device represents an easy of way of quantifying the growth of single and multiple cells. *S. cerevisiae* growth was monitored by counting the number of cells in the droplet and this requires imaging the droplets every time step. This droplet array represented growth of single cells in a batch mode and the device could be used to observe the increase of cell biomass with time. These studies can be used in combination with bulk culturing techniques to yield new insights in the field of bio-product optimization [15,16].

Furthermore, the device can be used to understand the impact of genetic changes on the growth rates in different media, and this can be used to identify and indicate the change in physiology. For example, FY2, YLH1 and YLH2, YLH3 and P1A2 could be studied in different media like YNB, YPD etc. and different environmental conditions. (Figure 27 and Table 9).

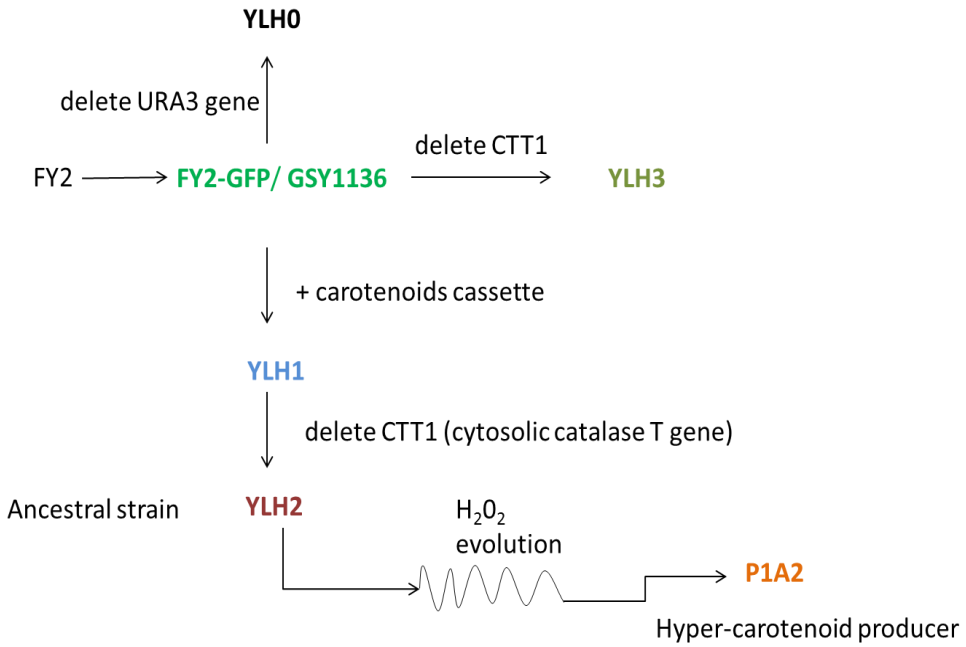

Figure 27. Diagrammatic representation of genotype of *S. cerevisiae.* FY2 is the wild type and P1A2/SM14 is the hyper-carotenoid producer. [51]

Table 9. Organism for future work. [13,51].

Organism	Strain	Genotype	Reference
S. cerevisiae	YLH0	GSY1136 ΔURA3	Reyes et al. , 2014
	YLH1	GSY1136::YIplac211YB/I/E	
	YLH2	GSY1136::YIplac211YB/I/E ΔCTT1	
	YLH3	GSY1136 ΔCTT1	

This platform even though useful, required much more manual work (cell encapsulation in the droplet, droplet storage, time lapse microscopy, and eventual cell counting using ImageJ) than would be preferred in a laboratory setup. This feature made the platform unattractive for extensive practical use. Investigating single-cell growth is

of fundamental importance to understand the heterogeneity of cellular growth [15]; but it is unlikely that this platform will be used in its current form. Automation of the imaging process, droplet generation and cell counting process needs to be achieved for a practical use of the device.

The thickness of the petri-dish with water in which the device is stored and thickness of thin PDMS layer at the bottom of device manifested as a challenge for brightfield and florescence microscopy of the cells. Quality of the images was significantly lower because of the additional optical distance between the microscope lens and the cells to be imaged. Also, transmitted light traveling through medium of different refractive indices (plastic petri-dish, water, thin PDMS layer and thick PDMS layer) and contributes to poor quality images and hinders the automation of imaging process. Hence, additional device modification would increase potential uses of the device. Additionally, alternate device design to integrate capability of re-cultivation of the cells and variable chemical composition in a droplet array are worth exploring.

In our studies we assumed the diffusivity of small molecules like carbon di-oxide, oxygen and water[33], and the diffusion of ions and media molecules was neglected. It is possible that ion and substrate diffusivity takes place from the thin PDMS later at the bottom and thus limits the availability of nutrients in the droplet. Growth results in droplets under the absence of such studies and characterization could lead to potentially misleading conclusion about growth results.

6.2 Perfusion chip for algal cells

Even though we employed multiple chambers to capture cells (=50) based on [53], most of the chambers had multiple cell or no cells, but very few single cells. This indicates a need to change the cell culture density introduced into the device. Here it is important to note that as a cell grows the cell size changes and the ratio of flow resistance changes (Table 10), which ultimately governs capture of cells in the trapping channel. Dewan et al [8] in their droplet-based study reported a smallest and largest cell size of 2.3 micron and 12.6 micron, respectively, an average cell size change from 5.99 micron (standard deviation=1.08) to 7.33 micron (standard deviation=1.3) from exponential growth phase to stationary growth phase, and a statistically significant change in cell size in the stationary phase. Yamamoto et al. reported *C. vulgaris* to measure 3 to 4 micron in diameter and its autosporangia are 6 to 8 micron in diameter [37]. In the light of significantly different cell dimensions, there arises a need to optimize the current device dimensions for a more effective cell capture. This could be achieved by decreasing the device depth which would force the cells to grow in single focal plane. It is important to note that the cells tend to grow in three dimensions and the flow ratio in Table 10 are sensitive to changes in this value.

Our study assumed a continuous exchange of nutrients based on the experiments of Rowat et al [53]. High cell density in the trapping channel during the growth of *C. vulgaris* could affect the flow pattern and hence the characterization of continuous flow through cells needs to be conducted for high density of algal cells in the channel. This could be done in similar manner as done by Rowat et al [53].

Table 10. Sensitivity of bypass to trapping channel flow rates to device dimensions. This table represents the sensitivity of $(Q_2/Q_1)_{\text{with cell}}$ as a function of the cell dimensions and height of the device for device dimensions shown in Figure and $(Q_2/Q_1)_{\text{without cell}}$=4.28.

h	**l_{1c}**	**w_{1c}**	**h_{1c}**	**$(Q_2/Q_1)_{\text{with cell}}$**
5	7	1	0.7	13.8
5	7	1	1	7.54
5	7	1	1.5	5.24
5	7	1.5	0.7	10.63
5	7	2	0.7	9.04
5	7	2	1	5.91
5	7	4	1.5	4.52
5	6	1	0.7	12.24
5	8	1	0.7	15.17
5	8	2	0.7	9.72
5	8	2	1	6.15
5	5	1	0.7	11.08
8	7	1	0.7	43.31
8	7	1	1	17.67
8	7	2	1	10.97
8	7	2	1.5	6.26
8	7	4	1.5	5.26
8	3	1	1	10.02

There is a great commercial interest in extra-and intra-cellular products of algal cells. Understanding the lipid heterogeneity of single algal cell has been of a special growing interest. This device could also be modified to understand the single cell heterogeneity of lipids and other extra-and intra-cellular products under perfusion and in

isolation from each other. Ref. [60] noted a cell to cell variation of lipids in the algal cells trapped in alginate droplets and reported no significant change in vitality of the cells captured in alginate droplet. However, a change in lipid content over time was not reported. Additionally, being trapped in a solidified alginate droplet presents an external mechanical stress to the cell and could impact the lipid production of cell. Ref [61] reported a droplet based device to understand the lipid change in single cells over time. Droplets are, however, not only limited by nutrient exchange but also by diffusion of small molecules (like water) in PDMS-based devices leading to a change in nutrient concentration over time. If the final results are not corrected for such effects, results might lead to misleading conclusions about the cell growth. A perfusion chip is thus an ideal candidate to investigate time-resolved heterogeneity in lipid contents in isogenic algal cells.

We propose that chip design in Figure 6 with device optimization and additional channel for cell staining and washing (Nile Red/BODIPY 505/515, [62]) and vitality (SYTOX Green, [60]) could potentially be used to understand the lipid content of algal cells over their growth. Additionally, the change in lipid content with media composition and irregularities in autospore number of algal cells, encountered under conditions of excess nutrients like sugar, peptone, and ammonium salts could be investigated ([38,63]). Understanding of these parameters would help understand when single cells in their growth cycle maximize lipid growth (or other product of interest) and thus providing a strategy to harvest cells for maximum product in an industrial scale culture.

6.3 Enzymatic etching

In our experiments we have demonstrated that we can successfully etch nano-channels. A critical aspect of the project that needs to be addressed and explored is the completion of the channels by bonding it to a flat surface of PLA. In the previous work by Huang et al.[30] the method used to created holes in the PLA using PDMS pillars. While trying to repeat this step in this work it was realized that this step is difficult to replicate and the area where the pillar is inserted into the mold for replication leads to surface unevenness. This consequently manifested in the flat PLA substrate not bonding well with the etched substrate (or the replicated channel). Drilling hole using a drill bit was explored as an alternative in this work, because of the ease of using the drilling process. This method, however, also experienced roughness and there were pockets of air around the region of holes. We hypothesized that the heat released from friction during the drilling process is enough to locally deform the material. This local deformation leads to improper contact between the area where the hole is drilled and the flat substrate, resulting in an air pocket. More experiments/alternate approaches would be needed to address this critical step for completion of the architecture for ultimate filtration application.

Additionally, the dimensions need to be optimized for an ultimate effective and high throughput separation. Computational Fluid Dynamic (CFD) studies to model the geometry validated with the separation experiments can help identify the optimized dimensions. Table 11 indicates some dimensions that could be tested. Specifically, it would be interesting to investigate the effect of the changing the widths of the channels

and the barrier to observe the effect of separation. Also, in previous study by Huang et al, it was shown that the separation depends upon the height difference of the two channels. As velocity is given by the flow rate divided by the cross-sectional area, it is speculated that in general area ratios would lead up to the velocity difference between the channels (velocity difference or pressure difference is the basis for the separation or transport of particles to move from one side of the barrier to the other). This can be studied by conducing separation experiments with various dimensions and can be validated with CFD modeling (Table 11).

Table 11. Device dimensions to be tested for separation of sub-micron particles.

W_1	W_2	W_b	h_1	h_2	h_b	R
(in microns)						
100	250	50	10	10	0.5	500
100	250	50	10	10	0.5	1000
100	450	75	10	10	0.5	500
100	450	75	10	10	0.5	1000

Once the geometric parameters have been optimized, a series and parallel combination of this architecture could be explored for high-throughput multi-component separations. For example, one could have use a series arrangement of these devices with a decreasing or increasing barrier depth for separation of particles of different sizes. Depending on the weir depth, this could find application to separate sub-micron particles

(like proteins/exosomes or other sub-cellular components of interest) from whole blood containing a mixture of cells of different sizes, cell debris, proteins etc.

7. CONCLUSIONS

We used PDMS-based static droplet array to investigate the growth rates of single and multiple cells of *Saccharomyces cerevisiae* in droplet. We observed an encapsulation efficiency of cells close to the random encapsulation efficiency. For single cell encapsulation, random encapsulation predicted 28.9% efficiency, and the observed encapsulation efficiency was 36.4%. The results are expected to follow random encapsulation for a large number of experiments. For the SM14 (P1A2) strain, we observed an average specific growth rate of 0.236 hr^{-1} in YNB media and for FY2-GFP strain we observed an average growth rate of 0.257 hr^{-1}. The results for the P1A2 strain from the droplet experiment matched with the results from the bioreactor run of the strains. For future work, we propose investigating the impact of genetic modifications and media composition on growth rate at single-cell level, as this information could be used to understand and quantify changes in cell physiology.

Additionally, we tested a device to understand the cell growth and cell division of single and multiple *Chlorella vulgaris* cells in a perfusion chip. Our preliminary observations correlated with the results and finding of growth and size of single algal cells in droplet of a previous study. With further device design modification, optimization (and introducing a cell staining and washing step) could be used for quantitatively and qualitatively understanding single cell growth and lipid heterogeneities.

Lastly, we employed enzymatic machining to etch nano- and micron sized channels on a biodegradable substrate, (poly lactic) acid. We obtained a characteristic etch rate of 1.45 μm h^{-1} and 0.16 μm h^{-1} for the poly(lactic acid) at 37 °C and 24.4 °C using the enzyme proteinase K. Consequently, a lower temperature of 24.4 °C (with etch rate of 0.16 μm h^{-1}) was favorable to etch sub-micron scale depth as only a small depth is etched for a given time compared to etching at higher temperature. Enzymatically etched channels separated by a weir of height in sub-micron range could be fashioned to separate sub-cellular components could be explored for separation of sub-cellular components like exosomes. In addition, CFD simulation studies would be able to give optimum geometric parameters for an effective high-throughput separation.

REFERENCES

1. Xia Y, Whitesides GM (1998) Soft lithography. Annual Review of Materials Science 28: 153-184.

2. Thorsen T, Maerkl SJ, Quake SR (2002) Microfluidic large-scale integration. Science 298: 580-584.

3. Unger MA, Chou H-P, Thorsen T, Scherer A, Quake SR (2000) Monolithic microfabricated valves and pumps by multilayer soft lithography. Science 288: 113-116.

4. Whitesides GM, Ostuni E, Takayama S, Jiang X, Ingber DE (2001) Soft lithography in biology and biochemistry. Annual Review of Biomedical Engineering 3: 335-373.

5. Yager P, Edwards T, Fu E, Helton K, Nelson K, et al. (2006) Microfluidic diagnostic technologies for global public health. Nature 442: 412-418.

6. Chin CD, Laksanasopin T, Cheung YK, Steinmiller D, Linder V, et al. (2011) Microfluidics-based diagnostics of infectious diseases in the developing world. Nature Medicine 17: 1015-1019.

7. Nguyen N-T, Wereley ST (2002) Fundamentals and applications of microfluidics, Second Edition (Integrated Microsystems). Artech House.

8. Dewan A, Kim J, McLean RH, Vanapalli SA, Karim MN (2012) Growth kinetics of microalgae in microfluidic static droplet arrays. Biotechnology and Bioengineering 109: 2987-2996.

9. Huang JH, Jayaraman A, Ugaz VM (2012) Enzymatic sculpting of nanoscale and microscale surface topographies. Angewandte Chemie International Edition 51: 9619-9623.

10. Metzger P, Largeau C (1999) Chemicals of *Botryococcus braunii*. Chemicals from microalgae.Taylor & Francis Inc. 10: 205-253.

11. Aldiguier A, Alfenore S, Cameleyre X, Goma G, Uribelarrea J, et al. (2004) Synergistic temperature and ethanol effect on *Saccharomyces cerevisiae* dynamic behaviour in ethanol bio-fuel production. Bioprocess and Biosystems Engineering 26: 217-222.

12. Steen EJ, Chan R, Prasad N, Myers S, Petzold CJ, et al. (2008) Metabolic engineering of *Saccharomyces cerevisiae* for the production of n-butanol. Microbial Cell Factories 7. doi:10.1186/1475-2859-7-36.

13. Reyes LH, Gomez JM, Kao KC (2014) Improving carotenoids production in yeast via adaptive laboratory evolution. Metabolic Engineering 21: 26-33.

14. Mitsuhashi S, Hosaka K, Tomonaga E, Muramatsu H, Tanishita K (1995) Effects of shear flow on photosynthesis in a dilute suspension of microalgae. Applied Microbiology and Biotechnology 42: 744-749.

15. Dusny C, Schmid A (2015) Microfluidic single-cell analysis links boundary environments and individual microbial phenotypes. Environmental Microbiology 17: 1839-1856.

16. Fritzsch FS, Dusny C, Frick O, Schmid A (2012) Single-cell analysis in biotechnology, systems biology, and biocatalysis. Annual Review of Chemical and Biomolecular Engineering 3: 129-155.

17. Schmid A, Kortmann H, Dittrich PS, Blank LM (2010) Chemical and biological single cell analysis. Current Opinion in Biotechnology 21: 12-20.

18. Deere D, Shen J, Vesey G, Bell P, Bissinger P, et al. (1998) Flow cytometry and cell sorting for yeast viability assessment and cell selection. Yeast 14: 147-160.

19. Oliver MH, Harrison NK, Bishop JE, Cole PJ, Laurent GJ (1989) A rapid and convenient assay for counting cells cultured in microwell plates: application for assessment of growth factors. Journal of Cell Science 92: 513-518.

20. Kuntanawat P, Ruenin J, Phatthanakun R, Kunhorm P, Surareungchai W, et al. (2014) An electrostatic microwell–based biochip for phytoplanktonic cell trapping. Biomicrofluidics 8: 034108. doi: 10.1063/1.4882196.

21. Kintses B, van Vliet LD, Devenish SR, Hollfelder F (2010) Microfluidic droplets: new integrated workflows for biological experiments. Current Opinion in Chemical Biology 14: 548-555.

22. Lagus TP, Edd JF (2013) High-throughput co-encapsulation of self-ordered cell trains: cell pair interactions in microdroplets. RSC Advances 3: 20512-20522.

23. Lagus TP, Edd JF (2012) High throughput single-cell and multiple-cell micro-encapsulation. Journal of Visualized Experiments 64: 4096. doi: 10.3791/4096.

24. Lee PJ, Hung PJ, Rao VM, Lee LP (2006) Nanoliter scale microbioreactor array for quantitative cell biology. Biotechnology and Bioengineering 94: 5-14.

25. Schmitz CH, Rowat AC, Köster S, Weitz DA (2009) Dropspots: a picoliter array in a microfluidic device. Lab on a Chip 9: 44-49.

26. Clausell-Tormos J, Lieber D, Baret J-C, El-Harrak A, Miller OJ, et al. (2008) Droplet-based microfluidic platforms for the encapsulation and screening of mammalian cells and multicellular organisms. Chemistry & Biology 15: 427-437.

27. Brouzes E, Medkova M, Savenelli N, Marran D, Twardowski M, et al. (2009) Droplet microfluidic technology for single-cell high-throughput screening. Proceedings of the National Academy of Sciences 106: 14195-14200.

28. Chang Y-W, He P, Marquez SM, Cheng Z (2012) Uniform yeast cell assembly via microfluidics. Biomicrofluidics 6: 024118. doi: 10.1063/1.4714421.

29. Falconnet D, Niemistö A, Taylor R, Ricicova M, Galitski T, et al. (2011) High-throughput tracking of single yeast cells in a microfluidic imaging matrix. Lab on a Chip 11: 466-473.

30. Boedicker JQ, Vincent ME, Ismagilov RF (2009) Microfluidic confinement of single cells of bacteria in small volumes initiates high-density behavior of quorum sensing and growth and reveals its variability. Angewandte Chemie International Edition 48: 5908-5911.

31. Au SH, Shih SC, Wheeler AR (2011) Integrated microbioreactor for culture and analysis of bacteria, algae and yeast. Biomedical Microdevices 13: 41-50.

32. Kim HS, Weiss TL, Thapa HR, Devarenne TP, Han A (2014) A microfluidic photobioreactor array demonstrating high-throughput screening for microalgal oil production. Lab on a Chip 14: 1415-1425.

33. Toepke MW, Beebe DJ (2006) PDMS absorption of small molecules and consequences in microfluidic applications. Lab on a Chip 6: 1484-1486.

34. Shim J-u, Cristobal G, Link DR, Thorsen T, Jia Y, et al. (2007) Control and measurement of the phase behavior of aqueous solutions using microfluidics. Journal of the American Chemical Society 129: 8825-8835.

35. Pan J, Stephenson AL, Kazamia E, Huck WT, Dennis JS, et al. (2011) Quantitative tracking of the growth of individual algal cells in microdroplet compartments. Integrative Biology 3: 1043-1051.

36. Wigmosta MS, Coleman AM, Skaggs RJ, Huesemann MH, Lane LJ (2011) National microalgae biofuel production potential and resource demand. Water Resources Research 47.

37. Yamamoto M, Nozaki H, Miyazawa Y, Koide T, Kawano S (2003) relationship between presence of a mother cell wall and speciation in the unicellular microalga *Nannochloris* (Chlorophyta). Journal of Phycology 39: 172-184.

38. Yamamoto M, Fujishita M, Hirata A, Kawano S (2004) Regeneration and maturation of daughter cell walls in the autospore-forming green alga *Chlorella vulgaris* (Chlorophyta, Trebouxiophyceae). Journal of Plant Research 117: 257-264.

39. Raposo G, Stoorvogel W (2013) Extracellular vesicles: exosomes, microvesicles, and friends. Journal of Cell Biology 200: 373-383.

40. Melo SA, Sugimoto H, O'Connell JT, Kato N, Villanueva A, et al. (2014) Cancer exosomes perform cell-independent microRNA biogenesis and promote tumorigenesis. Cancer Cell 26: 707-721.

41. Nguyen DG, Booth A, Gould SJ, Hildreth JE (2003) Evidence that HIV budding in primary macrophages occurs through the exosome release pathway. Journal of Biological Chemistry 278: 52347-52354.

42. Giri PK, Kruh NA, Dobos KM, Schorey JS (2010) Proteomic analysis identifies highly antigenic proteins in exosomes from *M. tuberculosis*-infected and culture filtrate protein-treated macrophages. Proteomics 10: 3190-3202.

43. Giri PK, Schorey JS (2008) Exosomes derived from *M. Bovis* BCG infected macrophages activate antigen-specific CD4+ and CD8+ T cells in vitro and in vivo. PloS one 3. doi: 10.1371/journal.pone.0002461.

44. World Health Organization (2014) Global tuberculosis control: WHO report 2014: World Health Organization. Hyperlink: http://apps.who.int/iris/bitstream/10665/137094/1/9789241564809_eng.pdf

45. Bhatnagar S, Schorey JS (2007) Exosomes released from infected macrophages contain *Mycobacterium avium* glycopeptidolipids and are proinflammatory. Journal of Biological Chemistry 282: 25779-25789.

46. Bhatnagar S, Shinagawa K, Castellino FJ, Schorey JS (2007) Exosomes released from macrophages infected with intracellular pathogens stimulate a proinflammatory response in vitro and in vivo. Blood 110: 3234-3244.

47. Dye C (2006) Global epidemiology of tuberculosis. The Lancet 367: 938-940.

48. Kruh-Garcia NA, Schorey JS, Dobos KM (2012) Exosomes: New Tuberculosis Biomarkers-Prospects from the Bench to the Clinic, Understanding Tuberculosis. InTech Open Access Publisher. doi:10.5772/30720.

49. Bithi SS, Vanapalli SA (2010) Behavior of a train of droplets in a fluidic network with hydrodynamic traps. Biomicrofluidics 4: 044110. doi: 10.1063/1.3523053.

50. Kao KC, Sherlock G (2008) Molecular characterization of clonal interference during adaptive evolution in asexual populations of *Saccharomyces cerevisiae*. Nature Genetics 40: 1499-1504.

51. Olson ML (2014) Metabolic Engineering of *S. cerevisiae* for carotenoid production optimization. Master's thesis, Texas A&M University.

52. Sun M, Bithi SS, Vanapalli SA (2011) Microfluidic static droplet arrays with tuneable gradients in material composition. Lab on a Chip 11: 3949-3952.

53. Rowat AC, Bird JC, Agresti JJ, Rando OJ, Weitz DA (2009) Tracking lineages of single cells in lines using a microfluidic device. Proceedings of the National Academy of Sciences 106: 18149-18154.

54. Kerls MN (2012) Simultaneous electricity, bioethanol, and algal biodiesel production using a microbial fuel cell. Master's thesis, Texas Tech University.

55. Kim J, Hegde M, Jayaraman A (2010) Co-culture of epithelial cells and bacteria for investigating host-pathogen interactions. Lab on a Chip 10: 43-50.

56. Kim J, Hegde M, Kim SH, Wood TK, Jayaraman A (2012) A microfluidic device for high throughput bacterial biofilm studies. Lab on a Chip 12: 1157-1163.

57. Kim J, Hegde M, Jayaraman A (2010) Microfluidic co-culture of epithelial cells and bacteria for investigating soluble signal-mediated interactions. Journal of Visualized Experiments 38: 1749. doi: 10.3791/1749.

58. Eddington DT, Puccinelli JP, Beebe DJ (2006) Thermal aging and reduced hydrophobic recovery of polydimethylsiloxane. Sensors and Actuators B: Chemical 114: 170-172.

59. Satyanarayana S, Karnik RN, Majumdar A (2005) Stamp-and-stick room-temperature bonding technique for microdevices. Journal of Microelectromechanical Systems 14: 392-399.

60. Lee D-H, Bae CY, Han J-I, Park J-K (2013) In situ analysis of heterogeneity in the lipid content of single green microalgae in alginate hydrogel microcapsules. Analytical Chemistry 85: 8749-8756.

61. Kim HS, Guzman AR, Thapa HR, Devarenne TP, Han A (2016) A droplet microfluidics platform for rapid microalgal growth and oil production analysis. Biotechnology and Bioengineering. doi:10.1002/bit.25930

62. Cooper MS, Hardin WR, Petersen TW, Cattolico RA (2010) Visualizing "green oil" in live algal cells. Journal of Bioscience and Bioengineering 109: 198-201.

63. Fott B, Nováková M (1969) A monograph of the genus *Chlorella*. The fresh water species. Studies in Phycology 50: 10-74.